Global and Planetary Change
October 2019, Volume 181, Pages 102988 (15p.)
https://doi.org/10.1016/j.gloplacha.2019.102988
https://archimer.ifremer.fr/doc/00506/61768/

The Messinian Ebro River incision

Pellen Romain [1, *], Aslanian Daniel [2], Rabineau Marina [1], Suc J.P. [3], Gorini C. [3], Leroux Estelle [2], Blanpied C. [3], Silenziario C. [4], Popescu S.M. [5], Rubino J.L. [6]

[1] Université de Bretagne Occidentale, IUEM, Domaines océaniques, UMR 6538 CNRS, 1 place Nicolas Copernic, 29280 Plouzané, France
[2] IFREMER, Laboratoire Géodynamique et enregistrements Sédimentaires, BP70, 29280 Plouzané, France
[3] Sorbonne Universités, UPMC University Paris 06, CNRS, Institut des Sciences de la Terre de Paris (iSTeP), UMR 7193, 4 place Jussieu, 75005 Paris, France
[4] ENI GAM-Schlumberger, Milano, Italy
[5] GeoBioStratData.Consulting, 385 route du Mas Rillier, 69140 Rillieux la Pape, France
[6] TOTAL, TG/ISS, CSTTF, Avenue Laribeau, 64018 Pau Cedex, France

* Corresponding author : Romain Pellen, email address : romain.pellen@univ-brest.fr

Abstract :

Morphological sills condition sedimentary, water and fauna exchanges between different domains. In particular, sills are crucial factors to consider during the Messinian Salinity Crisis (MSC) palaeogeographic evolution (5.97–5.33 Ma) of the NW Mediterranean area. Here we focus on the Ebro River and its up to now unexplained short Messinian onshore length (~100 km) compared to that of the Messinian Rhone River (~480 km) despite similar present-day drainage basins. Thanks to an extensive seismic and borehole dataset, we present a new interpretation of a complete 270 km long Messinian Ebro incised-valley system course underneath the present-day continental margin and bathyal basin and its related distal detrital deposits. These results favour a syn-MSC or pre-MSC opening of the (endorheic) Ebro Basin to the Mediterranean. We propose a mechanism of retrogressive erosional process, localized at structural knickpoints that shift seaward through time. This mechanism resulted in the development of the complete incised-valley system and the falling stage system tract (FSST) during the MSC sea level fall with negligible or even null retrogressive inland erosion beyond the Catalan Coastal Range. The shifting of erosion-deposition is controlled by the pre-Messinian stepwise morphology and segmentation in the Valencia, Menorca and Liguro-Provence Basins. By comparison, the Rhone system is simpler, characterized by the key role of a single knickpoint (at the shelf-break) and a steeper continental slope. Both cases highlight the relationship between kinematic, segmentation and their relative morphologies, base-level fall and erosional/depositional response particularly well expressed during the outstanding MSC associated with a huge relative sea-level drop that we measured down to -1100 m below present day sea-level.

Highlights

► Segmentation and differential subsidence highlighted in Pellen et al. (2016) control the Messinian palaeogeography ► A 270 km long Messinian palaeo-Ebro incised valley is recorded along the Valencia Basin.► Clastics related to the MSC erosion are deposited as FSST (in the Valencia Basin) and LST in Menorca Basin. ► Sediments of Tortonian, Messinian and Pliocene ages were drilled by the Benicarlo C1 well. ► The specific flat and stepped paleomorphology of the basin prevents onshore Messinian erosion in the Ebro Basin. ► The observed incision favors a *syn*-MSC or pre-Messinian opening model of the (endorheic) Ebro Basin to the Mediterranean Sea.

Keywords : NW Mediterranean Sea, Segmentation, Knickpoint, Ebro fluvial system, Messinian Salinity Crisis, Incised-valley system.

Abbreviations General

ESP Expended Spread Profile
Km Messinian Knickpoint
Ka Present-day knickpoint
MSC Messinian Salinity Crisis
Twt Two-Way Travel time

Geography

CCR Catalan Coastal Range
CFZ Central Fracture Zone
EB Ebro Basin

GOL Golf of Lion
LPB Liguro-Provence Basin
MB Menorca Basin
NBFZ North Balearic Fracture Zone
VB Valencia Basin

Stratigraphy

FAD First Appearence Datum
FSST Falling Stage System Tract
HST Highstand System Tract
LAD Last Appearence Datum
LST Lowstand System Tract
LU Lower Unit
MES Messinian Erosional Surface
MRS Maximum Regression Surface
MLM Messinian Lower Megasequence
MUM Messinian Upper Megasequence
MU Mobile Unit
RSME Regressive Surface of Marine Erosion
TST Transgressive System Tract
UU Upper Unit

1. Introduction

Morphological sills, whether related to sedimentary, inherited structural reliefs or originating from the kinematic history, play a crucial role in the sedimentary, water and fauna exchanges between basins through time. These sills often fit areas of different crustal nature and different subsidence histories, as observed in the Mediterranean-Paratethys area (e.g. Leever *et al.*, 2010; Leroux *et al.*, 2015a; Palcu *et al.*, 2017; Pellen *et al.*, 2017). In the case of huge relative sea-level variations, as during the MSC (5.97-5.33 Ma) (Manzi *et al.*, 2013), consideration of these barriers is of primary importance to understand the morphological and sedimentary evolution of the different basins (e.g. Leever *et al.*, 2010; Flecker *et al.*, 2015; Palcu *et al.*, 2017; Suc *et al.*, 2015; Balázs *et al.*, 2017).

1.1. The Ebro Paradox

The Rhone and Ebro fluvial systems are excellent examples of major rivers in the Mediterranean Sea (the 2nd and 3rd respectively after the Nile) that experienced the same crisis in response to the isolation of the Mediterranean Sea. Present-day drainage areas are of similar size (nearly 99,000 km^2 and 86,000 km^2, respectively) (Babault *et al.*, 2006) (Fig. 1). However direct comparisons between the Messinian palaeo-Ebro and Messinian palaeo-Rhone systems point out the so-called "Ebro paradox" (Babault *et al.*, 2006): despite similar present-day drainage areas, the length of the Messinian subaerial incision of the Ebro river seems much shorter than that of the Rhone river. In the case of the Messinian palaeo-Rhone, a total 480 km long fluvial incision network was described along the Alps (Clauzon, 1982, 1999) to the pre-Messinian Platform edge (Bache, 2008) (Fig. 1). In the case of the Messinian palaeo-Ebro erosion system, the incision is limited to about 100 km from the Catalan Coastal Range (CCR) edges to the former pre-Messinian platform edge (Fig. 1) (Urgeles *et al.*, 2011) with no major incision described in the endorheic Ebro Basin. Why such a difference? Babault *et al.* (2006) proposed that the Ebro River did not exist before the Messinian Salinity Crisis and that the connection between the endorheic Ebro Basin to the Mediterranean Sea occurred after the MSC (or potentially during this phase).

Conversely, several authors consider that seismic data provide evidence of well-developed sedimentation and deltaic progradation during the Tortonian and the development of a main incised-valley system during the MSC, implying a Tortonian connection between the Ebro Basin (EB) and the Valencia Basin (VB) (e.g. Cameselle *et al.*, 2014). Recent modeling and field

data on the foreland EB further argued that the transition from endorheic to exorheic of Ebro is pre-Messinian, although the precise timing remains to be established (12 to 7.5 Ma) (Fillon *et al.*, 2013; Garcia-Castellanos and Larrasoaña, 2015). However, the absence of major fluvial incision toward the onshore EB, the short incision of ~100 km and the absence of well-described detrital syn-MSC deposits in the VB remain unanswered. Indeed, Messinian clastic deposits were only partially described and mainly on the (present-day) outer shelf. These deposits were described either on top (Escutia and Maldonado, 1992; Maillard *et al.*, 2006a,b, or below the so-called Upper Unit (UU, Garcia *et al.*, 2011; Cameselle *et al.*, 2014, 2015) of the well-known Messinian trilogy (LU-MU-UU) synthetised by Lofi *et al.* (2011) (Fig. 1). This peculiar morphology strongly contrasts with that of the Western, Gulf of Lion, and Eastern, Nile region, Mediterranean that both show long fluvial system incisions and large detrital deposits during the Messinian sea-level fall (Gorini *et al.*, 2015) and remain to be explained.

1.2. Geodynamic and stratigraphic framework

The Neogene palaeoenvironmental framework of the NW Mediterranean region is largely condition by geodynamic history which controls the vertical motion and sedimentation in each sub-basin (Leroux *et al.*, 2015a, 2015b; Pellen *et al.*, 2016). The geometry and physical link between the evaporitic and detritic successions, and major tectonic hinge lines are well known in the Liguro-Provence Basin (LPB, Bache *et al.*, 2015; Leroux *et al.*, 2015a) (Fig. 1). However, a complete regional stratigraphic and morphological seismic tudy linking the CCR edges to the deep LPB is still lacking.

A NW-SE segmentation distinguishes the MB from the Mesozoic VB (Roca, 1992; Etheve *et al.*, 2016, 2018) and the deep LPB (Fig 1): the Central and North Balearic Fracture Zones (CFZ and NBFZ) represent two major sills that created a stepwise accommodation between the three domains (Pellen *et al.*, 2016). The geodynamic process leading to the formation of these sills is rooted in the counter-clockwise rotation of Corsica-Sardinia block during the early Miocene which drove the movement of Menorca Island, and non-kinematic motion of Ibiza-Majorca islands (Pellen *et al.*, 2016). These motions distinguish early Miocene LPB and MB basins from the Mesozoic VB basin (e.g. Olivet, 1996; Gueguen *et al.*, 1998; Bache *et al.*, 2010; Pellen *et al.*, 2016, Etheve et al., 2016). One of the main consequences is a different subsidence history for

each basin, with purely vertical Neogene "sag" subsidence for the Mesozoic VB (Pellen *et al.*, 2016).

A NW-SE segmentation shapes the GOL-LPB with five differentiated crustal domains on the French side (Moulin *et al.*, 2015; Afilhado *et al.*, 2015; Jolivet et al., 2015): unthinned continental crust, thinned continental crust, highly thinned continental crust, exhumed lower continental crust and proto-oceanic crust. Three domains of subsidence were found defined by three hinge lines (Fig.1, 2). On the platform and slope, the subsidence takes the form of a seaward tilt with different amplitudes, whereas the deep basin (with exhumed lower continental crust and proto-oceanic crust) subsides purely vertically (Leroux *et al.*, 2015).

The shelves of the MB and the GOL (domain 2a) (Fig. 1) first record a late Oligocene-Aquitanian marine influx (Roca and Guimera, 1992; Roca *et al.*, 2001; Bache *et al.*, 2010), followed by Burdigalian-Tortonian clay-marl then sand deposits associated with a prograding trend. The outermost position of this Tortonian shelf is shown on Figure 1 (from Bache, 2008). The deep part of the LPB and MB are usually associated with condensed Burdigalian-Tortonian deposits (Roca *et al.*, 2001). The Mesozoic VB (Roca, 1992; Etheve *et al.*, 2016, 2018) experienced the first marine ingression during the late Burdigalian-Langhian followed by an enhanced Tortonian prograding trend in the Tortosa area (Clavell and Berastegui, 1992; Cameselle *et al.*, 2014; Pellen *et al.*, 2016).

1.3. Ebro versus Rhone inheritances

The initiation of the endorheic sedimentation in the EB has been estimated at ~35 Ma (Costa *et al.*, 2010), the final preserved lacustrine fill -stage is proposed to be at least 13.5 and 12 Ma (in Urgeles *et al.*, 2011) and up to Tortonian (e.g. Vasquez-Urbez *et al.*, 2013). At the time of the basin's opening towards the Mediterranean Sea, an elevation of 535-750 m above sea level has been estimated (Garcia-Castellanos and Larrasoaña, 2015) which places the Catalan Coastal Range (CCR) as an important morphological barrier between the VB and EB. At the dawn of the MSC, a stepped morphology is observed for the VB-MB where offshore knickpoints are located at the edge of the Miocene platform or at major geodynamic boundaries (Fig. 2). On the contrary, the GOL is characterized by a single continental slope (Guennoc *et al.*, 2000). Furthermore, no major geodynamical sill is observed along the onshore Rhone drainage system (Séranne, 1999; Guennoc *et al.*, 2000; Sissingh, 2001).

In this study, based on a large set of seismic and borehole data, we made a detailed synthesis of the offshore physiography during Messinian, by correlating the VB, MB, and LPB with seismic stratigraphic and geomorphological methods tied to existing borehole data with revisited detailed biostratigraphic analysis to propose a new understanding of Ebro and Rhone systems evolution during the MSC.

2. Data and Method

2.1. Dataset

Our study is based on a large set of seismic and borehole data collected during the extensive French academia–industry programs (Actions-Marges, GRI Tethys Sud), in close collaboration with the Total and Schlumberger groups as well as data available from the Spanish SIGEOF database. This compilation provided for the correlation of seismic markers from the VB towards the LPB (as shown already in Pellen *et al.*, 2016). Twenty-four petroleum wells drilled between 1969 and 2004 along the NE Iberian margin have been used to calibrate seismic interpretations, although the stratigraphic information was often sparse or vague. We used The detailed stratigraphic, sedimentological and micropaleontological information available from three wells located on the present-day Ebro platform to constrain ages and palaeoenvironments of identified surfaces and units: Fornax 1 (Bailey *et al.*, 2008; Urgeles *et al.*, 2011; Cameselle *et al.*, 2014; Mauffrey *et al.*, 2017), Benicarlo C1 (this study) and Tarragona E2 (Evans *et al.*, 1978 ; Bessais & Cravatte, 1988).

In this paper the detailed lithological, environmental and biostratigraphic information from the Benicarlo C1 are provided for Miocene-Messinian-Pliocene series (based on Evans *et al.*, 1978) that we have revisited in the light of recent biostratigraphic charts, a modern geological time scale (Gradstein *et al.*, 2012) and correlation with more regional information (see chapters 3.2 to 4.2).

2.2. Sequence stratigraphy

Conventional seismic stratigraphic method was used (Mitchum & Vail, 1977; Vail *et al.*, 1977) to identify seismic discontinuities and stratigraphic surfaces and units based on reflexion configurations and facies characteristics (See the Table in Supplementary Material 3 for details of surfaces and units). However, identified surfaces and units were interpreted using principles

of sequence stratigraphy in their revised most recent version i.e. including interpretation of Falling Stage System Tract (FSST) (e.g. Hunt and Tucker, 1992; Catuneanu *et al.*, 2011), forced regression concept (e.g. Plint *et al.*, 1988) with Maximum Regression surface (MRS) and Regressive Surface of Marine erosion (RSME) (e.g. Helland-Hansen and Hampton, 2009). Ages of these sequences were provided by well data. Our interpretations were then integrated into the 'Kingdom Suite' software to insure coherency at all crossing lines. For the Messinian units, we used the now well established so-called « Messinian-trilogy »Lower Unit (LU)/Mobile Unit (MU)/ Upper Unit (UU) as synthesized by Lofi *et al.* (2011). Nevertheless, we provide special focus on units and sub-units related to clastic units (see results below).

.

2.3. Time to depth conversion and backstripping

Our seismic interpretations were converted from time to depth using average sediments velocities (layer cake model), to obtain the geometries in depths (meters) of surfaces and sedimentary units (Fig. 3, Transect01). Seismic velocities strongly vary in space within the same stratigraphic interval, with significant variations between the shelf, the base of slope, and the basin. Compiled borehole velocities on the VB platform and on the foot slope, as well as ESP velocities located in the deep LPB (Leroux *et al.*, 2016) were used to estimate an average velocity for each layer (see velocity model in suppl. mat. 1). The depth converted profile allowed us to measure the difference in altitudes between key points along the profiles, and sedimentary unit thicknesses.

A simple 2-D backstripping was performed to reconstruct geometries through time (in particular at early Zanclean, at Messinian low stand incised-system and related deposits (see details in suppl. mat. 2). Input parameters for the VB domain include paleobathymetry, age, and porosity of sedimentary packages based on Urgeles *et al.* (2011). An estimated total subsidence value up to 960 m/Ma for the deep LPB domain was also applied to the 2-D backstripping for Pliocene-Quaternary times as quantified by Rabineau *et al.*, (2014).

2.4. Knickpoint definition and chosen approach

Our study used the identification of knickpoints, highlighted either by morphological change or new sedimentary sequences development along the seismic profile. Different processes are

associated with onshore and offshore development of such morphological features. On land, knickpoints are interpreted as resulting from renewed erosion of a rejuvenated river that propagates upstream and influences the development of landscapes and source-to-sink systems (Grimaud *et al.*, 2016). They are usually triggered by a relative fall in river base-level (either through eustatic sea-level drop, tectonic faulting or uplift) and can also highlight the onshore-offshore position (Goswani *et al.*, 2016). Submarine knickpoints are often located at the shelf-break creating an offlap-break either (i) at the transition between the outer shelf and the continental slope (e.g. Rabineau *et al.*, 2014), or (ii) at the boundary of domains where tectonic motion displaces the seafloor (Amblas *et al.*, 2011) or (iii) at the site where channel levees are breached. Knickpoints are key elements to take into account in when considering segmented domains, we therefore paid a particular attention to their identification.

Below, we present our results from the onshore domain towards the deeper offshore domains.

3. Results

3.1. Morphology from seismic interpretation

Figure 3 presents our stratigraphic interpretation across the VB-MB along six seismic profiles perpendicular to the main erosional incision. Transect 01 has been converted to depth. Eight major seismic surfaces are illustrated, S0 (Tertiary basement), MES, S11, S20, S21, S22, S24, and S30 which respectively delimit four seismic units: SU12a-c, LU, MU and UU and three major knickpoints (Km1-3). Three secondary surfaces (S26a, b, c) are also identified in the UU. Relationships, age and interpretations of surfaces and units are presented in the table in suppl. mat. 3.

The first knickpoint Km_1 is located at the transition between the former foreland EB (~535 m above sea level) and the VB at the edges of the CCR (Figs. 2 and 3). Below this knickpoint, the Marginal Erosional Surface (MES, Lofi *et al.*, 2011) shows a highly rugged and dissected surface with frequent incisions organized in a dendritic pattern (also interpreted on 3D seismic data, e.g. Urgeles *et al.*, 2011, and Cameselle *et al.*, 2014) (Figs. 2 and 3, section a). Four palaeo-drainage systems are observed (Fig. 2) that present numerous incised fluvial tributaries with rough badland-like morphology of the MES (Urgeles *et al.*, 2011) above the isocontour of 1.6 sec TWT (~2.5 km depth) below present-day sea level. It is worth noting that the MES truncates the former Tortonian prograding clinoforms which form the Miocene platform in

the Tortosa-Ebro domain (Figs. 3 and 4). This is also confirmed by the Tarragona E2 well which sampled Tortonian deposits just below the MES (Bessais & Cravatte, 1988). A wide dentritic palaeo-drainage system is mapped for the Tortosa-Ebro domain (Fig. 2) which is the main and deepest NW-SE river channel interpreted as the Messinian Ebro fluvial system (Urgeles *et al.*, 2011) (Fig. 2, 3 section a & b). A ~61 km long main channel incision can be measured from the pre-MSC coast to the Tortosa-Ebro lower slope.

The erosive surface S11 extends seaward of the MES at the position of the Km_2 (Fig. 3, Transect01 - km 130; Fig. 4) at the Miocene platform edge, delimiting the base of SU12a showing downlapping prograding clinoforms geometries. Only the bottomset part of the clinoforms has been preserved on both sides of the main Messinian river channel. The basal erosive surface S11 also marks a change in the progradational trend along the Miocene platform edge (Fig.4, section h) of the Tarragona area: A major change in direction of sediment input from the morphological domain of Barcelona to the Tortosa-Ebro domain is highlighted by the basal erosive surface S11.

S11 shows a generally smoother morphology towards the VB foot-slope domain. In this area the MES subtracts into two erosive surface: the basal erosive surface S20 which truncate the seismic unit SU12a while the top erosive surface S30 bound the UU seismic unit (Fig. 3, sections c, d). Along the former Miocene outer shelf, the MES-S20 surface shows a smoother erosive surface below 2.5 km depth (Fig. 4, sections g, h) with the disappearance of badland morphology except in the axis of the main channel incision (Fig. 3, section b; Fig. 4). The extension of the S20 surface across the VB foot-slope domain highlights the lateral continuation of an incised channel along the VB domain. A slight NE-ward inclination is observed along the incised-valley profile with a mean present-day depth position ranging from 2.8 km below sea level at the Tortosa domain foot-slope to 3.2 km depth at its outlet (Fig. 3, sections c-f). The morphology shows an evolution from a ~6 km wide with an interfluve/thalweg height of 370-400 m at the toe of the proto-Ebro slope offshore the Tortosa-Tarragona domain (Fig. 3, sections a-c) to a ~16 km wide, 100-130 m deep incision at the transition towards the MB (Fig. 3, sections d, e). Bedrock morphology partly deflects the path of the incised-valley and slightly influences its sinuosity (Fig.2; Fig. 3, section c).

On both sides of this SW-NE valley, which totals a length of ~134 km in the deep VB domain, the surface is relatively conform compared to the underlying deposits. The main incised-valley

is joined by two smaller tributaries from the SW part of the VB and already mapped by Cameselle *et al.* (2015).

At the transition between the VB and MB (CFZ area in Figs. 2, 3 and 5, section i) (Maillard and Mauffret, 1999; Pellen *et al.*, 2016), S20 shows another knickpoint Km_3 (~3.2 km depth, at Transect01, km 270 in Fig. 3). It marks: **1)** the deepening of the basal surface S11 and its overlying unit SU12c – as the lateral correlation of SU12a; **2)** the last S20 toplap features; **3)** the formation of two new surfaces, S21 – as the lateral correlation of S20 – and S22 at the top and **4)** the thickening of the UU.

The S12 and S21 surfaces delimitates the development of SU12c with the NE-ward preserved prograding clinoforms (Fig. 5, section j). S21 at the top of SU12c also shows some widespread erosion and becomes smoother and conformable towards the MB-LPB transition (Fig. 3, section f). The conformable and non-incised S21 development also highlights the formation of the overlying LU. Both observations attest the termination of the trans-VB incised-system thus marking its outlet at the VB-MB transition.

The continuity of the erosional system from the VB platform to the Km_3 knickpoint therefore points to a 270 km long system that we identify as the trans-VB Messinian valley system (Figs. 2 and 3, Transect 01 and sections b-d). The MB-LPB transition marked by the North Balearic Fracture Zone (NBFZ) corresponds to the full development of the Messinian trilogy units (LU-MU-UU) as identified in the deep LPB domain (Figs. 3 and 9).

Using the backstripped section of Transect01 at 5.3 Ma (i.e. at the end of the MSC), we measure the general slope of the MES-S20-S21 from 90 to 430 km as equal to 0.55 % (i.e 0.32 °). However, individual segments in between knickpoints show a slope even smaller than 0.4 % (0.23°) and 0.45% (0.26°), between 90-280 km and 310-430 km respectively. Conversely, surface S11 at the base of SU12c shows a slope of 1.58% (0.9 °), between 310 and 430 km.

3.2. Borehole data

3.2.1. Biostratigraphy

The Benicarlo C1 well (Fig. 6) provided planktonic foraminifers recorded from cuttings (Evans *et al.*, 1978). These data have been re-visited and evaluated in light of the most recent biostratigraphic zonation in the Mediterranean (Iaccarino *et al.*, 2007) and the modern geological time scale (Gradstein *et al.*, 2012).

The top of Cretaceous limestones (Upper-Middle Cenomanian) is well identified at 4330 m depth. With respect to several Mediterranean long records (Suc *et al.*, 1992; Lirer and Iaccarino, 2011), the base of Pleistocene deposits (i.e. the base of the Gelasian, at 2.6 Ma) can be assessed between 2330 m depth (uppermost occurrence of *Sphaeroidinellopsis subdehiscens*, usually estimated at 3.2 Ma) and 2060 m (lowermost occurrence of *Globorotalia inflata*, dated at 2.09 Ma in the Mediterranean Sea; Iaccarino *et al.*, 2007). Consequently, our biostratigraphic re-evaluation focuses on the depth interval 4300–2300 m, which encompasses the Middle-Late Miocene and whole Pliocene (Fig. 6). Examining the vertical distribution of the species with a biostratigraphic significance along the studied interval, we paid particular attention to discontinuous occurrences, some punctual records may result from cavings or reworkings.
Orbulina universa is present from 4240 m depth that suggests an age younger than 14.10 Ma (First Appearance Datum, FAD, of the species in the Mediteranean; Iaccarino *et al.*, 2007). *Neogloboquadrina acostaensis* has been continuously recorded from 4240 to 4180 m, then intermittently at 3830 m, and continuously from 3710 m to 2040 m. The FAD of *N. acostaensis* in the Mediterranean Sea is dated at 11.90 Ma. Two interpretations can be discussed: (1) to place the FAD of *N. acostaensis* at 4240 m or (2) to place it at 3710 m. Hypothesis 1 implies very thick deposits to be ascribed to Tortonian while hypothesis 2 suggests that deposits from the base of the studied interval partly belong to the Serravallian and maybe to the Langhian. Caliper log (Fig. 6) suggests the presence of numerous caving effect between 3600 m and 4240 m which would affect the record of *N. acostaensis* or *Orbulina universa* below 3710 m. As well, the biostratigraphic interpretation of the nearby Tarragona E2 well (Cravatte, 1980; Bessais, 1984; Bessais & Cravatte, 1988) would be more consistent with the second hypothesis. Accordingly, sediments between 4240 and 3710 m depth could belong to a time-interval running from biozone MMi5 to biozone MMi10 (Fig. 6).

Above, the continuous occurrence of *Neogloboquadrina humerosa* is recorded from 3230 m. The FAD of *N. humerosa* is placed within biozone MMi12 (Iaccarino *et al.*, 2007), in agreement with the identification of this biozone in the Benicarlo C1 well (Fig. 6). A similar comment can be expressed for *Globigerinoides extremus*, which has been continuously recorded in the Benicarlo C1 well between 3220 m and 2900 m, that is also conceivable with the FAD of the species at the base of biozone MMi12 (Iaccarino *et al.*, 2007).

The occurrence of *Globorotalia conomiozea* from 3110 to 2640 m characterizes the MMi13 biozone ending at 5.97 Ma (Iaccarino *et al.*, 2007). Then, *Globorotalia margaritae* and *Spheroidinellopsis paenedehiscens* are recorded together from 2535 m, indicating the biozones MPl1-MPl2 up to the first record of *Globorotalia puncticalata* at 2511 m indicating the base of biozone MPl3 (Iaccarino *et al.*, 2007). Finally, the uppermost record of *Globorotalia margaritae* at 2370 m is used to delimit the top of biozone MPl3, dated at 3.80 Ma. These data are transferred to Fig. 6 where the ages of the biozone boundaries are also indicated according to Iaccarino *et al.* (2007). It is thus obvious that an important portion of the deposits drilled at Benicarlo C1, more precisely those between 3110 m and 2511 m depth, belongs to the pre-evaporitic phase of the Messinian.

3.2.2. Lithologies and Environments

The very thick sequence of volcanic tuffs and lavas between 4315 m - 3730 m were deposited in a fairly shallow marine environment during late Serravallian-Early Tortonian time as shown by the thin interbeds of soft limestones containing rare Amphistegina sp. and planktonic foraminifera (Evans *et al.*, 1978).

The sequence between 3695-3016 m, of Tortonian age is of open marine, outer sublittoral to bathyal nature. The onset of colder water conditions over this interval is shown by the presence of sinistral coiled specimens of *Globorotalia acostaensis* (since around 3400m) before the warmer Messinian period (Suc et al., 1995; Evans *et al.*, 1978).

The interval 2810-2525 m represents a shallowing upward phase, with the probable formation of underwater supra-littoral conditions at the top. The reduction in planktonic foraminifera and the upward coarsening of the sediments suggests a general shallowing of the basin at this time.

The interval between 2525 - 2500 m can be separated in two parts: the topmost part of this interval between approximately 2510 - 2500 m as well as interval 2525 - 2524 m contain thin beds of white algal limestone interbedded with white sandstone and yellow to ochre marl/claystone. The lower limestone contains anhydrite. Additionally, the occurrence of a single cyprid ostracod, algae and bryozoan in the 2515 and 2525-2520 m ditch cuttings sample is taken to indicate both a stratigraphic and environmental break at this level and possibly reflects the establishment of brakisch - non-marine conditions (Evans *et al.*, 1978).

The interval 2500 - 2370 m is characterized by soft, light grey calcareous shales and marls/claystone with minor sand stringers throughout. This interval is assigned to the Ebro Group, Early Pliocene, deposited in an open marine environment.

4. Discussion

4.1. Age assignment and sequence stratigraphy interpretation

Combining the results from seismic interpretation in correlation with biostratigraphy from Benicarlo C1 well, we consider that the Messinian is represented mostly by marine sediments from 3016 to 2525 m depths, i.e. 491 m in thickness with a shallowing upward trend (Fig. 6). The proximal to distal correlation of seismic units SU12a to SU12c (both topped by the MES-S20) also shows a downward-shift of uppermost surface (as seen on depth-converted seismic transect shown in Fig. 3 and in backstripped section (Supp. Material 2).

The MES(-S20) is depicted as the maximum regressive surface (MRS in the sense of Catuneanu *et al.*, 2011) and is located at 2525 m in the Benicarlo C1 well. This MRS (MES) would be dated at 5.6 Ma according to Clauzon *et al.* (1996, 2015) and CIESM (2008). The underlying Messinian sediments (SU12a and SU12c) therefore correspond to the remaining sediments of the Falling Stage System Tract (FSST). According to our seismic interpretation, the erosive surface at the base (S11) may correspond to the regressive surface of marine erosion during the falling stage of the MSC crisis, also described in Quaternary sequences related to 100 000 years cycles (Rabineau *et al.*, 2005). However, some early pre-MSC Messinian sediments seem to be preserved as biostratigraphic data suggest with the presence of *Globorotalia Cibaoensis* around 3000 m but considering the relative Messinian sea level fall velocity and amplitude, earlier pre-MSC deposits are very fortunate to be reworked and preserved in MSC related deposits.

This interpretation of the FSST for SU12a is supported by the fact that Benicalo C1- shows sediments of a younger age than those found in both Fornax-1 and Tarragona E2 wells (Evans *et al.*, 1978 ; Bessais & Cravatte, 1988; Urgeles *et al.*, 2011) as well as a progressive downward shift of MES-S20 surface. Our seismic interpretation and correlation suggest that SU12c is also part of this FSST and in fact represent the end of it with the most distal regressive deposits. Development of SU12c unit is followed by the initiation of the LU as lowstand system tract (in

the sense of Boyd *et al.*, 2006; Gorini *et al.*, 2015) (Fig. 8, stage 3). This FSST and LST would correspond to the MLM (Messinian Lower Megasequence) of Gorini *et al.* (2015).

Unfortunately, no well exists to sample this unit SU12c, so we have no direct related biostratigraphic information, which could confirm or invalidate this hypothesis.
Above the MES at Benicarlo C1, the occurrence of a single cyprid ostracod, algae and brozoan in the 2515 m and 2525-2520 m cuttings suggest that this thin unit going from probable emersion to shallow water environments records the end of the MSC. Following CIESM (2008) or Bache *et al.*, (2012) scenarios, this unit could be interpreted as corresponding to those deposited during the early marine reflooding of the Mediterranean Basin (Transgressive System Tract) that preceded the base of the Zanclean, and estimated between 5.46 - 5.33 Ma. This TST is overlain by a clear open-marine high stand System Tract (HST) with warm conditions in early Zanclean Pliocene. (5.33-3.85 Ma) (Suc *et al.*, 1995).

4.2. Subaerial versus submarine erosion and position of the Messinian shoreline

Erosional surfaces may develop in subaerial or submarine environments. However, process and formation of erosional surfaces differ in the air and under water, due to the varying physics of the different fluids. In subaerial environments topography is highly variable. Landscapes are carved by rivers and strongly dependent on precipitation that will erode and transport sediment as a function of gravity and slopes as the primary controls. In submarine environments, widespread erosion also occurs: both in proximal environments (at the shoreline and on the shelf) with a strong impact of waves, tides and currents but also in deep environments such as submarine canyons, slopes and deep-sea areas with processes such as turbidity currents, landslides, debris flows (e.g. Amblas *et al.*, 2006) and contour currents (e.g. Rebesco *et al.*, 2014). In shallow environments (between 0 to 100 - 150m) a very efficient erosion process is related to wave action. The main result of this wave action is the creation of large smooth morphologies and wave-cut terraces that are recognized worldwide throughout the geological time scale (e.g. Cattaneo and Steel, 2003; Catuneanu 2006; Bache *et al.*, 2014).

In our case study, S11 marks the first MSC regressive surface of marine erosion (RSME) prior to the MES development (see also above) and highlights Km_2 at an onshore-offshore position (Goswami *et al.*, 2017). The overlying U12a clinoforms (VB area) correspond to the

Messinian forced-regressive prisms (FSST), with erosion and redeposition of sediments in the forced-regressive prisms (Fig. 4, section g; Fig. 6) and a MRS at the top.

The subaerial development of the Trans-VB incised-valley system is attested across the Tortosa-Ebro domain with rugged badland-type morphology, terraces, fluvial meanders, oxidation surfaces (Fornax-1) as fully explained in (Urgeles *et al.*, 2011; Cameselle *et al.*, 2014).

Moreover, as shown is the results section: the general slope of backstripped MES-S20-S21 erosional surface is only 0.55% (0.32°) or even less in segments between knickpoints (0.23° to 0.26 °). These slope gradients are much smaller than any present-day well-defined submarine canyon. In the GOL, the shelf-break occurs when slope gradients reach 1%. Gradients < 1% delimit the continental shelf, whereas gradients > 1% correspond to the upper slope. The values obtained for the Messinian MES-S20-S21 are typical of low shelf gradients and not slope gradients where submarine canyons occur, they are generally between 2 and 5 ° in canyon head areas in the GOL (Baztan *et al.*, 2005). Another example is provided by present-day submarine canyons in the VB that all show slopes around 10° in upper slope submarine canyons to 2-4° at the base of slope canyons (Amblas *et al.*, 2006). Those values are more than one order of magnitude higher that what we measured here. MES-S20 general shape cannot be related to any submarine canyon mechanism.

If MES-S20 might have been also initiated as submarine one, this composite erosive surface was then re-worked as a subaerial surface of erosion related to the Messinian lowermost sea level (MRS) with a coastline that reached at least km_3 (270 km; Fig. 3 Transect 01). Its outlet is associated with the development of SU12c after the Km_3 knickpoint and the start of S11c erosional surface at its base. The limit of prograding SU12c unit would thus correspond to the most distal detritic products related to the relative MSC sea level fall stage.

The Messinian shoreline (Fig. 3 Transect01; Fig. 5, section I and Supp. Mat 2) existed at least up to km 270. In any event, the minimum lowest MSC sea level (at km_3) was around -1100 m below present day sea-level according to the backstripped section, SU12c corresponds to the final development of the detritic product related to the MSC sea-level fall. The values we give here for sea-level reconstruction are probably maximum values as backstripping was conducted up to 5.3 Ma after the UU deposition (and not 5.6 Ma at the maximum sea level drawdown).

4.3. A model for the Messinian Ebro incised-valley formation: Segmentation, knickpoint role, and palaeogeographic implications.

The model in Fig. 7 attempts to explain the Ebro paradox and the following scenario, which highlights the multiple versus single knickpoint model implication in the fluvial dynamic during relative sea-level change. From this simplified model, identification of a 270 km long Messinian Ebro incised-valley system and its infilling by detrital FSST deposits allows us to propose an explanation clarifying the relationship between drainage areas and the Messinian fluvial incision.

The existence of a pre-Messinian physiography and segmentation in the Valencia Basin (Pellen *et al.*, 2016) plays a crucial role in its subsidence history, with an induced pre-Messinian step-by-step seafloor deepening between the sagged VB, the MB and the deep LPB (Figs. 7 & 8a, stage 1).

Prior to the MSC sea level fall, the gradual restriction of the marine connections (CIESM, 2008; Roveri *et al.*, 2014) would imply relative minor sea level variation. As a fact a first retrogressive erosion Km_1 is located at the CCR area, following the principle of the river equilibrium profile (Miall, 2013). The result is the initiation of S11 basal erosive surface at the platform edge (Km_2) (Fig. 8a, Stage 1) and the detrital sediment deposition (SU12a) offshore fluvial systems.

The progressive limitation of exchanges followed by the abrupt break of water exchanges through the Rifian strait (Krijgsman *et al.*, 1999) at 5.60 Ma resulted in a rapid sea-level fall within the Mediterranean Basin. The sea level quickly reached Km_2 (Fig. 8a, Stage 2a) implying a shift to the outermost limit of the Miocene platform of the main retrogressive erosion. The eroded products were gradually deposited along the former Miocene slope area, forming the SU12a unit (as drilled in Benicarlo well and showing ages of at least 6.14 to 5.72 Ma). With the sea-level fall continuing, up to 5.6 - 5.45 Ma depending on the chronostratigraphy of the discussed scenarios (i.e. CIESM, 2008; Bache et al., 2012, 2015; Gorini et al., 2015), the main regressive erosion shifted again and the upper part of S12a was partially reworked and redeposited in the offshore domain as in FSST or Forced regression models (Gorini *et al.*, 2015). Little detrital SU12a formation is observed at the VB base of slope because, between stage 2a and 2b (Fig. 8a), the accommodation space in the Valencia foot slope area was too small to accumulate thick series. This implies intense sedimentary transfer from the subaerial

eroded platform domain directly to the deep marine Menorca and Provence domains. When the sea level reached Km_3, the fluvial base-level and main retrogressive erosion migrated to the Valencia-Menorca transition with clear erosional truncations (Fig. 8a, stage 2b) and the detrital sedimentation was transferred to the Menorca and Provence deep domain, as shown by the development of the SU12c prograding clinoforms. At the lowest sea-level, our interpretations locate the shoreline at Km_3, observed on the CFZ axis (Fig. 3).

This evolution of downward shift erosion and the clear shift of the depocentres towards the deep basin is typical of a falling stage system tract that occurs on rather flat areas separated by steps which involve a proximal regressive erosion together with a distal retrogressive erosion at the step (knickpoint). As the sea-level fall continues, we observe a quick shift of this double erosion from Km_1 to Km_3. With this mechanism, the river equilibrium profile has to be well developed at Km_3 so as to observe major retrogressive erosional process at Km_2 area. Depending of the inertia of the retrogressive erosion dynamics at each knickpoint, there is no increased fluvial erosion nor propagation towards the onshore Ebro areas as in the case of the Rhône (see below). The existence of the CCR may also further prevent the propagation of the fluvial erosion towards the inner parts of the EB.

In the Rhone system, earlier work showed the existence of three hinge lines in between different structural domains related to the opening of the LPB. The model in Fig. 8b (stage 1-4) illustrates the development of Messinian Pyrenean-Languedocian and Rhone fluvial systems during the MSC sea-level drop, based on the work of Bache *et al.* (2009, 2010, 2012, 2015) and Gorini *et al.* (2015). Domain 2b corresponds to the main geodynamic sill which records the gradual transition between marine and aerial domain during the MSC sea-level fall (5.6-5.55 Ma) i.e. Gorini *et al.*, 2015) and slow sea-level rise (formation of wave ravinement erosion surface between 5.55-5.46 Ma if we fellow Bache *et al.*, 2012 scenario). Only minor onshore knickpoints are mapped along the Rhone fluvial profile (Clauzon, 1982), and the main knickpoint is therefore located at the hinge line 2 (the shelf-break) which also corresponds to the first development of forced falling stage system tract of the MSC (Leroux *et al.*, 2015a, b). The model highlights the initiation of retrogressive erosion at the second geodynamic knickpoint (the shelf break), which quickly progresses landward from the former Miocene shelf-edge to the edge of the Central Massif (Pyrenean-Languedocian rivers) or along the Rhone-Bresse valley (Fig. 8b, stage 1-3) up to Lyon city.

Domain 2a (GOL) can be compared to the VB basin area/VB-MB transition, which records the lowest MSC base-level and early relative sea-level rise. Around the Km3 area, a minimum of four successive marine incisions are observed in the UU deposits (Fig. 3, section e), implying (1) a composite refilling for the trans-VB valley system and (2) preservation of the latter in the sense of Boyd *et al.*, (2006). If the UU are mainly developed along the main channel (~0.3 twt thick) few deposits are observed on both sides of the channel, involving a partial/complete reshaping of S20 erosional surface. This observation may be related to other morphological features, such as the general extent of the smooth surface along the Catalan and domain 2b of the LPB (Bache *et al.*, 2009, 2012; Garcia *et al.*, 2011; this study) (Fig. 6). This tends to favour a similar genesis during a relative slow sea-level rise (Fig. 8, stage 4), the rough surface being eroded by wave action (Cattaneo and Steel, 2003; Bache *et al.*, 2012, 2015) and only preserved upstream by the later rapid sea-level rise closing the Messinian event.

We thus propose that domain 2b and VB basin area/VB-MB transition are equivalent morphological domains which both record the lowest MSC sea-level. Significant lateral spacing between each morphological knickpoint has provided better stratigraphic and morphological observation for the VB. As the VB record the whole Messinian palaeo-Ebro incised valley, the Ebro paradox disappears if the length of Messinian rivers are measured from MSC paleo-shorelines at the CFZ area, and not from pre-Messinian or present-day shorelines (Fig. 7).

At the MSC paroxysm, the trans-VB incised valley system watershed would include the Valencia Basin and its borders (55 000 km^2; including the Betic-influenced southwest area, its mountainous borders (southern part of the Catalan Range) and at least the eastern part of the Ebro Basin (? < Ebro watershed < 85 000 km^2). However, our result cannot confirm or infirm a pre-Messinian proto-Ebro hypothesis. Stratigraphic and thermochronological interpretations path suggest a pre-Messinian opening of the Ebro Basin (Fillon *et al.*, 2012; Cameselle *et al.*, 2013) with a single proto-Ebro river or multiple mountainous rivers cutting across the CCR. These models need to be confirmed by an assessment of offshore sedimentary volumes during Miocene, Messinian and Pliocene-Quaternary times that would lead to a better estimate of the paleo-drainage area evolution before/after the opening of the EB.

The NBFZ sill is overloaded by igneous pulses starting during the LU deposition and during Pliocene-Quaternary time (Fig. 8; this was also observed onshore by Marti *et al.*, 1992; Araña *et al.*, 1983). Recent studies have linked this Messinian magmatic pulse to the Messinian desiccation (Sternai *et al.*, 2017) or to a more global kinematic re-organization (Leroux *et al.*,

2018). Whatever the lithospheric processes implied, the Ebro incised-fluvial system constrained by the CCR and by the CFZ confirms the strong influence of VB-MB-LPB margin structural segmentation on the development of the Messinian Ebro fluvial system, and more generally on the whole Neogene sedimentological evolution.

5. Conclusion

Extending the Cameselle *et al.* (2014) results, we have identified and characterized along the Valencia, Menorca and towards Liguro-Provence basins a 270 km long Messinian fluvial valley-incision – from the Messinian shoreline to the CCR - as well as the spatial distribution of the related distal detrital deposits. The Ebro Messinian erosional system now displays the same order of incised river length as the Rhone, resolving the paradoxal relationship between the present-day fluvial drainage area and the Messinian fluvial system of Babault *et al.*, (2006). Following our interpretation, the Ebro Basin and Mediterranean Sea were connected at least at the MSC sea-level drop. Only detailed sedimentary fluxes analysis could confirm or infirm a pre-Messinian connection between the Ebro Basin and the Mediterranean Sea.

The segmentation and nature of the substratum triggered the formation of knickpoints due to differential subsidence between the shallow VB, the transitional MB and the deep LPB, and controlled fluvial processes and erosion during the MSC sea-level drop. These knickpoints induced step-by-step major regressive-retrogressive fluvial erosional processes which shift through time during sea-level drop. This work highlights the general major relationship between kinematic, subsidence evolution, base-level fall and depositional response particularly well expressed during the outstanding Messinian Salinity Crisis event.

Acknowlegments

This work was co-funded by a grant from the French government under the program "Investissements d'Avenir" the "Laboratoire d'Excellence" LabexMER (ANR-10-LABX-19), and ISBLUE *(ANR-17-EURE-0015)* and by a grant from the Regional Council of Brittany. It was further supported by CNRS and IFREMER, with additional support from the French Actions-Marges program (JL Rubino & P. Unternehr) and the GRI Méditerranée (Groupement Recherche et Industrie TOTAL-UPMC). The Data base was built thanks to the SIGEOF spanish site, to academic cruises from France including PROGRES, AMED-SARDINIA, SEEPGOL, VALSIS) and Spain. Additional industrial seismic lines were provided by

Schlumberger. The biostratigraphic studies and re-evaluations were performed by biostratigraphers from TOTAL. The authors acknowledge the fruitful and constructive reviews by Antonio Pedrera, Agnes Maillard and two anonymous reviewers, as well as those from the editor Liviu Matenco that greatly improved the manuscript.

References

Afilhado, A., Moulin, M., Aslanian, D., Schnürle, P., Klingelhoefer, F., Nouzé, H., Rabineau, M., Leroux, E., and Beslier, M.-O., 2015. Deep crustal structure across a young passive margin from wide-angle and reflection seismic data (The SARDINIA Experiment) – II. Sardinia's margin. Bulletin de la société géologique de france, 186, 331-351.

Amblas, D., Canals, M., Urgeles, R., Lastras, G., Liquete, C., Hughes-Clarke, J.E., Casamor, J.L., Calafat, A.M., 2006. Morphogenetic mesoscale analysis of the northeastern Iberian margin, NW Mediterranean Basin. Marine Geology 234, 3-20.

Amblas, D., Gerber, T.P., Canals, M., Pratson, L.F., Urgeles, R., Lastras, G., and Calafat, A.M., 2011. Transient erosion in the Valencia Trough turbidite systems, NW Mediterranean Basin. Geomorphology, 130 (3-4), 173-184.

Araña, V., Aparicio, A., Martin Escorza, C., Garcia Cacho, L., Ortiz, R., Vaquer, R., Barberi, F., Ferrara, G., Albert, J., and Gassiot, X., 1983. El volcanismo neogeno-cuaternario de Catalunya: caracteres estructurales, petrologicos y geodinámicos. Acta Geologica Hispanica, 28, 1-17.

Arche, A., G. Evans, and Clavell, E., 2010. Some considerations on the initiation of the present SE Ebro river drainage system: Post- or pre-Messinian? Journal of Iberian Geology, 36 (1), 73-85.

Babault, J., Loget, N., Van Den Driessche, J., Castelltort, S., Bonnet, S., Davy, P., 2006. Did the Ebro basin connect to the Mediterranean before the Messinian salinity crisis? Geomorphology, 81, 155-165.

Bache, F., 2008. Evolution Oligo-Miocène des marges du micro océan Liguro-Provençal. Thèse d'Etat. Université de Bretagne Occidentale, Brest, 1-328.

Bache, F., Olivet, J.L., Gorini, C., Aslanian, D., Labails, C., Rabineau, M., 2010. Evolution of rifted continental margins: the cases of the Gulf of Lions (western Mediterranean basin). Earth and Planetary Science Letters, 292, 345-356.

Bache, F., Gargani, J., Suc J.-P., Gorini, C., Rabineau, M., Popescu, S.M., Leroux, E., Do Couto, D., Jouannic, G., Rubino, J.-L., Olivet, J.-L., Clauzon, G., Dos Reis, A., and Aslanian, D., 2015. Messinian evaporite deposition during sea level rise in the Gulf of Lion (Western Mediterranean). Marine and Petroleum Geology, 66, 262-277.

Bache, F., Popescu, S.-M., Rabineau, M., Gorini, C., Suc, J.-P., Clauzon, G., Olivet, J.-L., Rubino, J.-L., Melinte-Dobrinescu, M.C., Estrada, F., Londeix, L., Armijo, R., Meyer, B.,

Jolivet, L., Jouannic, G., Leroux, E., Aslanian, D., Dos Reis, A.T., Mocochain, L., Dumurdžanov, N., Zagorchev, I., Lesić, V., Tomić, D., Çağatay, M.N., Brun, J.-P., Sokoutis, D., Csato, I., Ucarkus, G., Çakir, Z., 2012. A two-step process for the reflooding of the Mediterranean after the Messinian Salinity Crisis. Basin Research, 24, 125–153.

Bache, F., Sutherland, R., and King, PR., 2014. Use of ancient wave-ravinement surfaces to determine paleogeography and vertical crustal movements around New Zealand. New Zealand Journal of Geology and Geophysics 57, 459-467.

Bailey, H.W., Gallagher, L., Woodhouse, B., 2008. Biostratigraphy of the Well Fornax-Offshore, Spain, 12 pp. Unpublished biostratigraphic report.

Balázs, A., Granjeon, D., Matenco, L., Sztanó, O., Cloetingh, S., 2017. Tectonic and climatic controls on asymmetric half-graben sedimentation: inferences from 3-D numerical modelling. Tectonics, 36, 2123-2141.

Bartrina, M.T., Cabrera, L.L., Jurado, M.J., Guimera, J., and Roca, E., 1992. Cenozoic evolution of the central Catalan margin (Valencia Trough, Western Mediterranean). Geology and Geophysics of the Valencia Trough, Western Mediterranean. Tectonophysics, 203, 219–248.

Baztan, J., Berné, S., Olivet, J.-L., Rabineau, M., Aslanian, D., Gaudin, M., Réhault, J.-P., and Canals, M., 2005. Axial incision: the key to understand submarine canyon evolution (in the western Gulf of Lion). Marine and Petroleum Geology, 22 (6-7), 805-826.

Bessais, E., 1984. Etude palynologique du Pliocène du sondage Tarragona E2. Rapport de stage D.E.A. Univ. Sc. Tech. Languedoc, Montpellier, 21 pp.

Bessais, E. and Cravatte, J., 1988. Pliocène Vegetational ecosystems in South Catalonia, latitudinal variations in the Northwest Mediterranean Region. Geobios, 21, 49-63.

Boyd, R., Dalrymphe, R.W., and Zaitlin, B.A., 2006. Estuarine and Incised-Valley facies model. SEPM special publication, 84, 171-235.

Cameselle, A.L., Urgeles, R., De Mol, B., Camerlenghi, A., and Canning, J.C., 2014. Late Miocene sedimentary architecture of the Ebro Continental Margin (Western Mediterranean): implications to the Messinian Salinity Crisis. International Journal of Earth Science (Geol Rundsch), 1-18.

Cameselle, A.L., and Urgeles, R., 2015. Large- scale margin collapse during Messinian early sea- level drawdown: the SW Valencia trough, NW Mediterranean. Basin Research, 29 (S1), 576-595.

Canals, M., Casamor, J.L., Lastras, G., Monaco, A., Acosta, J., Berné, S., Loubrieu, B., Weaver, P.P.E. and Grehan, A., 2004. The role of canyons in strata formations. Oceanography, 17 (4), 81-91.

Canals et al., 2013. Integrated study of Mediterranean deep canyons: novel results and future challenges. Progress in Oceanography, 118, 1-27.

Cattaneo, A. and Steel, R.J., 2003. Transgressive deposits: a review of their variability. Earth-Science Reviews, 62, 187-228.

Catuneanu, 2006. Principles of sequence stratigraphy. Amsterdam, The Netherlands, Elsevier. 375 pp.

Catuneanu, O., Galloway, W.E., Kendall, C.G.S.C., Miall, A.D., Posamentier, H.W., Strasser, A., Tucker, M.E., 2011. Sequence stratigraphy: methodology and nomenclature. Newslett. Stratigr. 44 (3), 173-245.

CIESM, 2008. The Messinian Salinity Crisis from mega-deposits to microbiology – A consensus report. N° 33 in CIESM Workshop Monographs (F. Briand, Ed.), CIESM Publisher, Monaco, 168 pp.

Clauzon, G., 1982. Le canyon Messinien du Rhône : une preuve décisive du "desiccated deep-basin model" (Hsü, Cita and Ryan, 1973). Bull. Soc. Géol. Fr., 24 (3), 597-610.

Clauzon, G., 1999. L'impact des variations eustatiques du bassin de Méditerranée occidentale sur l'orogène alpin depuis 20 Ma (In French). Etudes Géogr. Phys., 28, 33–40.

Clauzon, G., Suc, J.-P., Gautier, F., Berger, A., Loutre, M.-F., 1996. Alternate interpretation of the Messinian salinity crisis: Controversy resolved? Geology, 24, 363–366.

Clauzon, G., Suc, J.-P., Do Couto, D., Jouannic, G., Melinte-Dobrinescu, M.C., Jolivet, L., Quillévéré, F., Lebret, N., Mocochain, L., Popescu, S.-M., Martinell, J., Doménech, R., Rubino, J.-L., Gumiaux, C., Warny, S., Bellas, S.M., Gorini, C., Bache, F., Rabineau, M., Estrada, F., 2015. New insights on the Sorbas Basin (SE Spain): The onshore reference of the Messinian Salinity Crisis. Marine and Petroleum Geology, 66, 71–100.

Clavell E. and Berastegui X., 1991. Petroleum geology of the Gulf of València. Generation, accumulation, and production of Europe's hydrocarbons (Ed. A.M. Spencer), Special Publication of the European Association of Petroleum Geoscientists, 1, 355-368.

Costa, E., Garcés, M., Lopez-Blanco, M., Beamud, E., Gomez-Paccard, M., and Larrasoaña, J. C., 2010. Closing and continentalization of the South Pyrenean foreland basin (NE Spain): magnetochronological constraints. Basin Research, 22, 904-917.

Cravatte, J., 1980, Etude microstratigraphique du Miocène et essai de corrélations entre les forages de Te-2, Garraf 1, BMB-1, BMC-1 et BME-1: Rapport confidentiel, total Direction fonctionnelle Exploration, département Laboratoires Exploration, p. 1-16.

Del Olmo, W.M., 2011. The Messinian in the Gulf of Valencia and Alboran Sea (Spain): paleogeography and paleoceanography implications. Revista de la Sociedad Geológica de España, 24, 1-22.

Do Couto, D., 2014. Evolution geodynamique de la Mer d'Alboran par l'étude des bassins sédimentaires. Thèse de doctorat de l'Université Pierre et Marie Curie, 554 pp.

Escutia, C., Maldonado, A., 1992. Paleogeographic implications of the Messinian surface in the Valencia trough, northwestern MediterraneanSea. In: Banda, E., Santanach, P. (Eds.), Geology andGeophysics of the Valencia Trough, Western Mediterranean. Tectonophysics, 203, 263–284.

Etheve, N., Frizon de Lamotte, D., Mohn, G., Martos, R., Roca, E., and Blanpied, C., 2016. Extensional vs contractional Cenozoic deformation in Ibiza (Balearic promontory, Spain): Integration in the West Mediterranean back-arc setting. Tectonophysics, 682, 35-55.

Etheve, N., Mohn, G., Frizon de Lamotte, D., Roca, E., Tugend, J., and Gomez-Romeu, J., 2018. Extreme Mesozoic Crustal thinning in the eastern Iberia margin: the example of the Columbrets basin (Valencia trough). Tectonics, 37 (2), 636-662.

Evans, D.J., Peter, C.K., Price, R.J., 1978. Biostratigraphy and depositional environments over the internal 450 m to 4492 m (T.D.), together with petrographic descriptions of samples between 3620 m to 4190 m in the Union Texas Espana Inc. Benicarlo C-1 well, offshore Spain, Robertson Research (North America) Limited, unpublished Exploration Report n° 194, 61 pp.

Fidalgo-Gonzàlez, L., 2001. Kinematic evolution of the North Atlantic ocean: implication of the intraplate deformation. Thèse de doctorat de l'Université de Bretagne Occidentale, Brest, 1-477.

Fillon, C., Gautheron, C., and van der Beek, P., 2013. Oligocene–Miocene burial and exhumation of the Southern Pyrenean foreland quantified by low-temperature thermochronology. Journal of the Geological Society, 170, 67-77.

Flecker, R., Krijgsman, W., Capella, W., de Castro Martins, C., Dmitriev, E., Mayser, J.P., Marzocchu, A., Modestu, S., Ochoa, D., Simon, D., Tulbure, M., van der Berg, B., ven der Schee, M., de Lange, G., Ellam, R., Govers, R., Gutjah, M., Hilgen, F., Kouwenhoven, T.J., Lofi, J., Meijer, P., Sierro, F.J., Bachiri, N., Barhoun, N., Alami, A.C., Chacon, B., Flores, J.A., Gregory, J., Howard, J., Lunt, D., Ochoa, M., Pancost, R., Vincent, S., and Yousfi, M.Z., 2015. Evolution of the Late Miocene Mediterranean–Atlantic gateways and their impact on regional and global environmental change. Earth-Science Reviews, 150, 365-392.

Frey-Martinez, J., Cartwright, J.A., Burgess, P.M., and Vicente-Bravo, J., 2004. 3D seismic interpretation of the Messinian Unconformity in the Valencia Basin, Spain: 3D Seismic Technology: Application to the Exploration of Sedimentary Basins. (Ed. by R.J. Davies, J.A. Cartwright, S.A. Stewart, M. Lappin & J.R. Underhill). Memoirs of the Geological Society, London, 29, 91-100.

Garcia, M., Maillard, A., Aslanian, D., Rabineau, M., Alonso, B., Gorini, C., and Estrada, F., 2011. The Catalan margin during the Messinian Salinity Crisis: Physiography, morphology and sedimentary record. Marine Geology, 284, 158-174.

Garcia-Castellanos, D., and Larrasoaña, J.C., 2015. Quantifying the post-tectonic topographic evolution of closed basins: The Ebro basin (northeast Iberia). Geology, 43 (8), 663-667.

Gorini, C., Montadert, L., and Rabineau, M., 2015. New imaging of the salinity crisis: Dual Messinian lowstand megasequences recorded in the deep basin of both the eastern and western Mediterranean. Marine and Petroleum Geology, 66, 1-17.

Goswani, R., Mitchell, N.C., Brocklehurst, S.H. and Argnani, A., 2016. Linking subaerial erosion with submarine geomorphology in the western Ionian Sea (south of the Messina Strait), Italy. Basin Research, 29, 641-658.

Gradstein, F.M., Ogg, J.G., Schmitz, M.D., Ogg, G.M., (eds.) 2012. The Geological Time Scale 2012, Elsevier, Amlsterdam, 1144 pp.

Grimaud, J.-L., Paola, C. and Voller, V., 2016. Experimental migration of knickpoints: influence of style of base-level. Earth-Surface Dynamics, 4, 1-11.

Gueguen, E., Doglioni, C., and Fernandez, M., 1998. On the post-25 Ma geodynamic evolution of the western Mediterranean. Tectonophysics, 298, 259-269.

Guennoc, P., Gorini, C., and Mauffret, A., 2000. Histoire géologique du Golfe du Lion et cartographie du rift oligo-aquitanien et de la surface messinienne. Géologie de la France, 3, 67-97.

Helland-Hansen, W. & Hampson, G. 2009. Trajectory analysis: concepts and application. Basin Research, 21 (5), 454-483.

Hunt, D. and Tucker, M. E., 1992. Stranded parasequences and the forced regressive wedge systems tract: deposition during base-level fall, Sedimentary Geology, 81, 1-9.

Iaccarino, S., Premoli Silva, I., Biolzi, M., Foresi, L.M., Lirer, F., Turco, E., Petrizzo, M.R., 2007. Practical manual of Neogene planktonic foraminifera. Biolzi, M., Iaccarino, S., Turco, E., Checconi, A., Rettori, R., eds., Univ. Perugia-Parma-Milano, 131 pp.

Jolivet, L., C. Gorini, Smit, J., and Leroy, S., 2015. Continental breakup and the dynamics of rifting in back-arc basins: The Gulf of Lion margin. Tectonics 34 (4): 2014TC003570.

Koss, J.E., Ethridge, F.G., Schumm, S.A., 1994. An experimental study of the effects of base-level change on fluvial, coastal plain and shelf systems. Journal of Sedimentary Petrology, 64, 90-98.

Krijgsman, W., Langereis, C.G., Zachariasse, W.J., Boccaletti, M., Moretti, G., Gelati, R., Iaccarino, S., Papani, G., and Villa, G., 1999. Late neogene evolution of the Taza–Guercif Basin (Rifian Corridor, Morocco) and implications for the Messinian salinity crisis. Marine Geology, 153, 147–160.

Leever, K.A., Matenco, L., Garcia-Castellanos, D., and Cloetingh, S., 2010. The evolution of the Danube gateway between Central and Eastern Paratethys (SE Europe): Insight from numerical modelling of the causes and effects of connectivity between basins and its expression in the sedimentary record. Tectonophysics, 502, 175-195.

Leroux, E., Aslanian, D., Rabineau, M., Granjeon, D., Gorini, C., and Droz, L., 2015a. Sedimentary markers in the Provençal Basin (western Mediterranean): a window into deep geodynamic processes. Terra Nova, 27, 122-129.

Leroux, E., Rabineau, M., Aslanian, D., Gorini, C., Bache, F., Moulin, M., Pellen, R., Granjeon, D., and Rubino, J.-L., 2015b. Post-rift evolution of the Gulf of Lion margin tested by stratigraphic modelling. Bulletin de la Société Géologique de France, 186, 291-308.

Leroux, E., Aslanian, D., Rabineau, M., Pellen, R., and Moulin, M., 2018. The late Messinian event: a worldwide tectonic upheaval. Terra Nova, 30 (3), 207-214.

Lirer, F., Iaccarino, S., 2011. Mediterranean Neogene historical stratotype sections and Global Stratotype Section and Points (GSSP): state of the art. Ann. Naturhist. Mus. Wien, 113(A), 67-144.

Lofi, J., Sage, F., Deverchère, J., Loncke, L., Maillard, A., Gaullier, V., Thinon, I., Gillet, H., Guennoc, P., and Gorini, C., 2011. Refining our knowledge of the Messinian Salinity crisis records in the offshore domain through multi-site seismic analysis. Bulletin de la Société Géologique de France, 182, 163-180.

Lofi, J., Camerlenghi, A., Aloisi, G., -Maillard, A. Garcia-Castellanos,D., Huebscher, C., Kuroda, J., 2017. The DREAM IODP project to drill the Mediterranean Salt Giant on the balearic promontary, EGU.

Maillard, A., Mauffret, A., 1999. Crustal structure and rift genesis of the Valencia Trough (NW Mediterranean Sea). Basin Research, 11, 357-379.

Maillard, A., Mauffret, A., 2006a. Relationship between erosion surfaces and Late Miocene Salinity Crisis deposits in the Valencia Basin (Northwestern Mediterranean): evidence for an early sea-level fall. Terra Nova, 18, 321–329.

Maillard, A., Gorini, C., Mauffret, A., Sage, F., Lofi, J., Gaullier, V., 2006b. Offshore evidence of polyphase erosion in the Valencia Basin (Northwestern Mediterranean): scenario for the Messinian Salinity Crisis. Sedimentary Geology, 188–189, 69–91.

Manzi, V., Gennari, R., Hilgen, F., Krijgsman, W., Lugli, S., Roveri, M., and Siorro, F.J., 2013. Age refinement of the Messinian salinity crisis onset in the Mediterranean. Terra Nova, 25, 315-322.

Marti J., Mitjavila, J., Roca, E., Aparicio, A., 1992. Cenozoic magmatism of the Valencia through (western Mediterranean): relationship between structural evolution and volcanism. Tectonophysics, 203, 145-165.

Mauffrey, M-A., Urgeles, R., Berné, S., Canning, J., 2017. Development of submarine canyons after the Mid-Pleistocene Transition on the Ebroi margin, NW Mediterranean: The role of fluvial connections, Quaternary Science Reviews, 158, 77-93.

Miall, A.D., 2013. The Geology of Fluvial Deposits, 4th corrected printing, 581 pp.

Mitchum R. & Vail P., 1977. Seismic stratigraphy and global changes of sea-level, part 7: Seismic Stratigraphic Interpretation Procedure - In Seismic Stratigraphy - Applications to hydrocarbon exploration; Payton C. E. (ed.): AAPG Mem. 26, Tulsa, Oklahoma, USA.

Moulin, M., Klingelhoefer, F., Afilhado, A., Aslanian, D., Schnurle, P., Nouzé, H., Rabineau, M., Beslier, M.-O., and Feld, A., 2015. Deep crustal structure across a young passive margin from wide-angle and reflection seismic data (The SARDINIA Experiment) – I. Gulf of Lion's margin. Bulletin de la Société Géologique de France, 186, 309-330.

Olivet, J.L., 1996. La cinématique de la plaque Ibérique. Bulletin des Centres de Recherches Exploration-Production Elf-Aquitaine, 20, 131-195.

Palcu, D.V., Golovina, L.A., Vernyhorova, Y.V., Popov, S.V., and Krijgsman, W., 2017. Middle Miocene paleoenvironmental crises in Central Eurasia caused by changes in marine gateway configuration. Global and Planetary Change, 158, 57-71.

Pellen, R., Aslanian, D., Rabineau, M., Leroux, E., Gorini, C., Silenziario, C., Blanpied, C., and Rubino, J.-L., 2016. The Menorca Basin: a buffer zone between the Valencia and Liguro-Provençal Basins (NW Mediterranean Sea). Terra Nova, 00, 1-16.

Pellen, R., Popescu, S.-M., Suc, J.-P., Melinte-Dobrinescu, M.C., Rubino, J.-L., Rabineau, M., Marabini, S., Loget, N., Casero, P., Cavazza, W., Head, M.J., and Aslanian, D., 2017. The Apennine foredeep (Italy) during the latest Messinian: Lago Mare reflects competing brackish and marine conditions based on calcareous nannofossils and dinoflagellate cysts. Geobios, 50 (3), 237-257.

Plint A. G., 1988. Sharp-based shoreface sequences and "offshore bars" in the Cardium Formation of Alberta: their relationship to relative changes in sea level - In Sea-level changes : an integrated approach ; Wilgus C. K., Hastings B. S. Et al. : SEPM Special Publication No. 42, Tulsa: p.357-370.

Rabineau, M., Berné,S., Aslanian, D., Olivet J-L., Joseph, P, Guillocheau, F, Bourillet, J-F., Ledrezen, E., Granjeon, D., 2005 : Sedimentary sequences in the Gulf of Lions : a record of 100,000 years climatic cycles, Marine and Petroleum Geology, 22, 775-804.

Rabineau, M., Leroux, E., Bache, F., Aslanian, D., Gorini, C., Moulin, M., Molliex, S., Droz, L., Reis, T.D., Rubino, J.-L., and Olivet, J.-L., 2014. Quantifying subsidence and isostatic readjustment using sedimentary paleomarkers, example from the Gulf of Lion. Earth and planetary Science Letters, 388, 1-14.

Rebesco, M., Hernandez-Molina, F.J., Van Rooij, D., and Wahlin, A., 2014. Contourites and associated sediments controlled by deep-water circulation processes: state-of-the-art and future considerations. Marine Geology, 352 (1), 111-154.

Roca, E., 2001. The Northwest Mediterranean Basin (Valencia Trough, Gulf of Lion and Liguro-Provençal basins): structure and geodynamic evolution. Peri-Tethyan Rift/Wrench Basins and Passive margins, 186 (Ed. by P.A. Ziegler, W. Cavazza, A.H.F. Robertson & S. Crasquin-Soleau), pp. 671-706. Peri-Tethys Memoir 6, Mémoires du Museum National d'Histoire Naturelle, Paris.

Roca E. and Guimerà J., 1992. The Neogene structure of the eastern Iberian margin: structural constraints on the crustal evolution of the Valencia trough (western Mediterranean). Tectonophysics, 203, 203-218.

Roure, F., Choukroune, P., Berastegui, X., Munoz, J.A., Villien, A., Matheron, P., Bareyt, M., Seguret, M., Camara, P., and Deramond, J., 1989. ECORS deep seismic data and balanced cross sections: geometric constraints on the evolution of the Pyrenees. Tectonics, 8, 41-50.

Roveri, M., Flecker, R., Krijgsman, W., Lofi, J., Lugli, S., Manzi, V., Sierro, F.J., bertini, A., Camerlenghi, A., De Lange, G., Govers, R., Hilgen, F.J., Hübscher, C., Meijer, P.T., and Stoica, M., 2014, The Messinian Salinity Crisis: Past and future of a great challenge for marine sciences: Marine Geology, 352, 25-58.

Séranne, M., 1999. The Gulf of Lion continental margin (NW Mediterranean) revisited by IBS: an overview. in Durand, B., Jolivet, L., Horvath, F., and Seranne, M., eds., The Mediterranean Basins: Tertiary Extension within the Alpine Orogen, Volume 156, Special publication, Geological Society of London, p.15-36.

Sissingh, W., 2001. Tectonostratigraphy of the West Alpine Foreland; correlation of Tertiary sedimentary sequences, changes in eustatic sea-level and stress regimes. Tectonophysics, 333, 361-400.

Slingerland, R., and Smith, N.D., 2004. River avulsions and their deposits. Annual Review of Earth and Planetary Sciences, 32, 257-285.

Stampfli, G.M., and Hoëcker, C.F.W., 1989. Messinian palaeorelief from a 3D seismic survey in the Tarraco concession area (Spanish Mediterranean Sea). Geologie en Mijnbouw, 68, 201-210.

Sternai, P., Caricchi, L., Garcia-Castellanos, D., Jolivet, L., Sheldrake, T.E., and Castelltort, S., 2017. Magmatic pulse driven by sea-level changes associated with the Messinian salinity crisis. Nature Geoscience, 10, 783-787.

Suc, J.-P., Bertini, A., Combourieu-Nebout, N., Diniz, F., Leroy, S., Russo-Ermolli, E., Zheng, Z., Bessais, E., and Ferrier J., 1995. Structure of West Mediterranean vegetation and climate since 5.3 Ma. Acta zool. Cracov., 38 (1), 3-16.

Suc, J.-P., Clauzon, G., Bessedik, M., Leroy, S., Zheng, Z., Drivaliari, A., Roiron, P., Ambert, P., Martinell, J., Doménech, R., Matias, I., Julià, R., Anglada, R., 1992. Neogene and Lower Pleistocene in Southern France and Northeastern Spain. Mediterranean environments and climate. Cahiers Micropaléontol., 7 (1-2), 165-186.

Suc, J.-P., Popescu, S.-M., Do Couto, D., Clauzon, G., Rubino, J.-L., Melinte-Dobrinescu, M.C., Quillévéré, F., Brun, J.-P., Dumurdzanov, N., Zagorchev, I., Lesic, V., Tomic, D., Sokoutis, D., Meyer, B., Macalet, R., and Rifelj, H., 2015. Marine gateway vs. fluvial stream within the Balkans from 6 to 5 Ma. Marine and Petroleum Geology, 66, 231-245.

Urgeles, R., Camerlenghi, A., Garcia-Castellanos, D., De Mol, B., Garcés, M., Vergés, J., Haslamk, I., and Hardmank, M., 2011. New constraints on the Messinian sea level drawdown from 3D seismic data of the Ebro Margin, western Mediterranean. Basin Research, 23, 123-145.

Vail, P.R., Mitchum, R.M., Todd, J.R.G., Widmier, J.M., Thompson, S., Sangree, J.B., Bubb, J.N., Hatlelid, W.G., 1977. In: Payton, C.E. (Ed.), Seismic stratigraphy and global changes of sea level: Seismic Stratigraphy – Applications to Hydrocarbon Exploration. Mem. Am. Ass. Pertol. Geol., 26, 49–212.

Vasquez-Urbez, M., Arenas, C., Pardo, G., and Pérez-Rivarés, J., 2013. The effect of drainage reorganization and climate on the sedimentologic evolution of intermontane lake systems: the final fill stage of the Tertiary Ebro Basin (Spain). Journal of Sedimentary Research, 83, 562-590.

Figures

Fig.1. A Present-day NW Mediterranean physiographic areas **and** previously published major physiographic features and seismic units assigned to the Messinian event (compiled from Stampfli and Hoëcker, 1989; Frey-Martinez *et al.*, 2004; Maillard *et al.*, 2006a, b; Del Olmo, 2011; Garcia *et al.*, 2011; Urgeles *et al.*, 2011; Bache *et al.*, 2009, 2015). Major geodynamic boundaries are represented in the Valencia-Menorca Basin (VB-MB): C.F.Z. = Central Fracture Zone; N.B.F.Z. = North Balearic Fracture Zone) (Maillard and Mauffret, 1999; Pellen *et al.*, 2016) and in the Liguro-Provence Basin (LPB): domain 1 = Unthinned Continental Crust; domain 2a = Thinned Continental Crust.; domain 2b = Highly thinned Continental Crust; domain 3 = Exhumed lower crust; domain 4 = Atypical oceanic crust) (Moulin *et al.*, 2015; Leroux *et al.*, 2015).

Fig.2. Map showing our new interpretation of the sedimentary units and main morphological observations associated to the Messinian event in the VB-VM. The Messinian drainage network (in red) could be followed from the shelf to the VB and up to the MB. Position of vertical sections a to f shown in black (see Fig. 3).

Fig.3. Seismic sections a-f showing the morphological evolution of the trans-VB Messinian valley system, its outlet and the related Messinian detrital and evaporitic deposits. The red marker symbolizes MES and S20 rough surface, the violet markers symbolize the smoother S21 surface at the outlet of the valley system. Transect01 is a composite dip section converted in depth (see methods and supplementary figures for more details) from the VB to the deep LPB. Note in particular the progressive downward shifts of top of units 12a and 12c). Position of the profiles is given in Fig. 2.

Fig. 4. Detailed seismic sections (sections g, h) highlighting the development of the Tortonian-Messinian shelf.

Fig. 5. Detailed seismic section highlighting the erosional truncations at the transition between the VB and the MB domain (section i) and development of the progradational seismic units SU12c in the deep and distal MB area (section j). We interpret this SU12c unit as the LST related to the MSC, it corresponds to the most distal progradating detritic unit observed in the area.

Fig. 6. Correlation of seismic units and Well Benicarlo C1, for the Miocene to Pliocene deposits. (Borehole position is shown on Figure 1 & 2). The right part of the figure shows the vertical records of the concerned species, the horizontal lines indicate which level has been

considered as corresponding to the first or last appearance datum (FAD or LAD) of some of them. Biozones and related ages refer to Gradstein *et al.* (2012). Caliper (blue curve) and Gamma Ray (red curve) are represented.

Fig.7. Simplified schematic section illustrating the role of multiple versus single knickpoints in retrogressive erosion response during a relative sea level fall. **a, b, c** correspond to the rejuvenation phase of the retrogressive erosion linked to the relative sea level successive falls (step 1, 2, 3).

Fig.8. Schematic and balanced cross section of the VB-MB and LPB (modified from Bache, 2008) illustrating the impact of sills and sea-level drop on the fluvial valley system development and paleo-depositional profile process during the Messinian event. During sea-level drop, erosion occurs both as regressive erosion of the fluvial system but also as retrogressive erosion from more distal knickpoints (see text for further explanation).

Fig.9. Detailed seismic section highlighting the magmatic pulse during the Lower Unit deposition and Pliocene-Quaternary time at the Menorca Basin and Liguro-Provence Basin transition (North Balearic Fracture Zone area) (Location and units color code as in Figs. 4 & 5).

SUPPLEMENTARY MATERIAL

Supplementary material 1. A) Time-depth velocity model used for the time to depth conversion of the Transect01 using velocity information from boreholes (Benicarlo C1, Bocarte 1, Castellon G1, Tarragona D2 and Fornax 1) and ESP refraction data in the VB and GOL.

Supplementary material 2. Backstripping reconstruction along the regional Transect01 profile (in depth). Input parameters for the VB domain include palaeobathymetry, age, and porosity of sedimentary packages based on Urgeles *et al.* (2011). Rabineau *et al.* (2014) presented a new method to quantify post-rift subsidence by direct use of sedimentary geometries. An estimated total subsidence value up to 960 m/Ma for the deep LPB domain was estimated for Pliocene and Quaternary times (Rabineau *et al.*, 2014) and applied to the 2-D backstripping. MES, S20 and base of Halite surfaces were reported on Fig. 3. Q1, Q2, P1 and P2 are respectively dated at 0.9, 1.8, 2.49 and 3.2 Ma following Urgeles *et al.* (2011) and Leroux *et al.* (2015b) studies.

Supplementary material 3. Summary of key seismic surfaces and units mapped across VB, MB, and LPB areas in this study. Unit age estimation are from Bache et al. (2015) and Gorini et al. (2015).

Supplementary material 4. Short video illustrating the evolution of sea-level and paleogeographies in the VB, MB and LPB between 6 and 5.20 Ma (using Placa 4D©ifremer software).

Highlights

- Segmentation and differential subsidence highlighted in Pellen et al. (2016) control the Messinian palaeogeography
- A 270 km long Messinian palaeo-Ebro incised valley is recorded along the Valencia Basin.
- Clastics related to the MSC erosion are deposited as FSST (in the Valencia Basin) and LST in Menorca Basin.
- Sediments of Tortonian, Messinian and Pliocene ages were drilled by the Benicarlo C1 well.
- The specific flat and stepped paleomorphology of the basin prevents onshore Messinian erosion in the Ebro Basin.
- The observed incision favors a syn-MSC or pre-Messinian opening model of the (endorheic) Ebro Basin to the Mediterranean Sea.

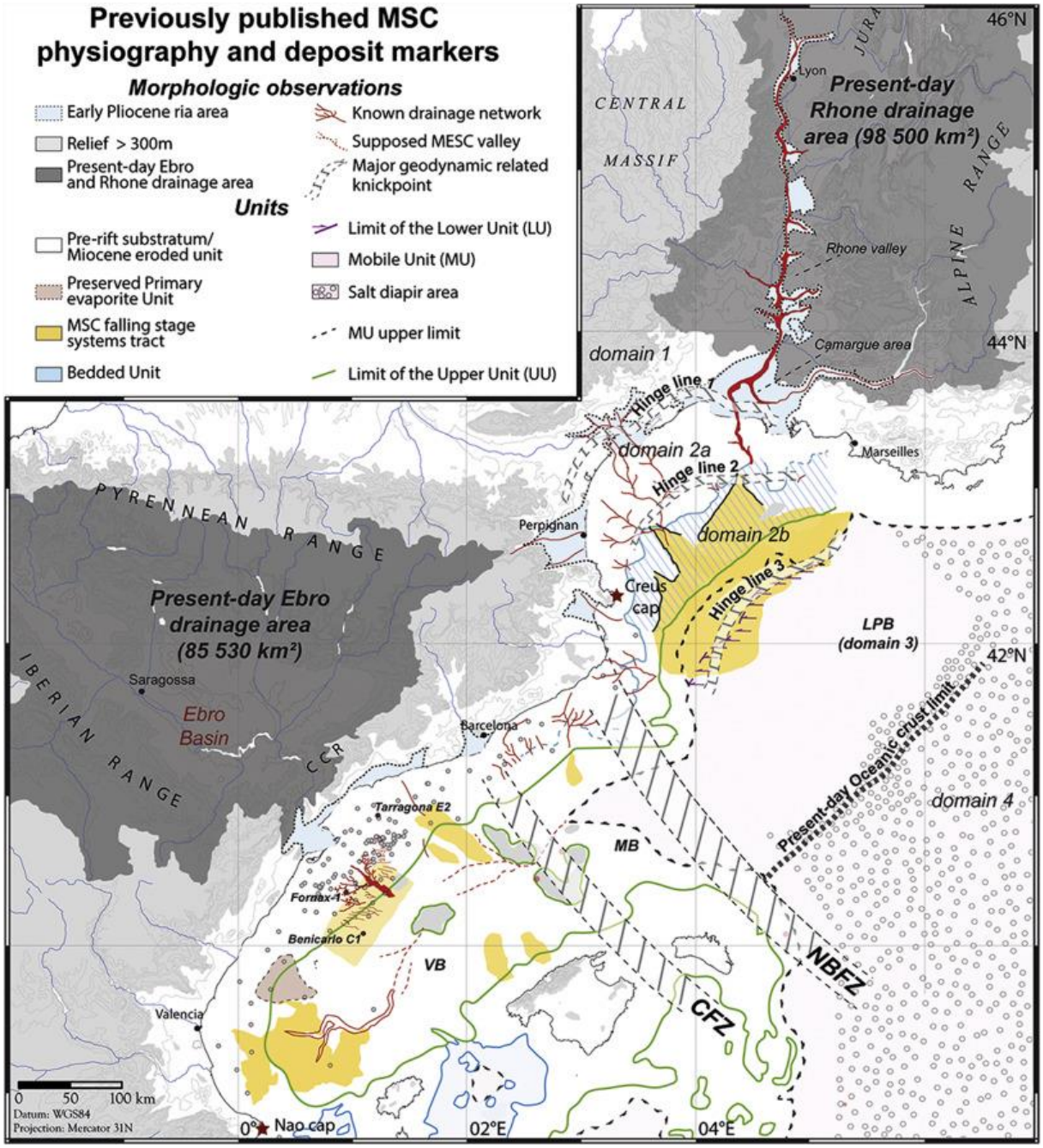
Previously published MSC physiography and deposit markers
Morphologic observations
Early Pliocene ria area
Relief > 300m
Present-day Ebro and Rhone drainage area
Known drainage network
Supposed MESC valley
Major geodynamic related knickpoint
Units
Pre-rift substratum/ Miocene eroded unit
Preserved Primary evaporite Unit
MSC falling stage systems tract
Bedded Unit
Limit of the Lower Unit (LU)
Mobile Unit (MU)
Salt diapir area
MU upper limit
Limit of the Upper Unit (UU)
46°N
JURA
CENTRAL MASSIF
Lyon
Present-day Rhone drainage area (98 500 km²)
ALPINE RANGE
Rhone valley
Camargue area
44°N
domain 1
Hinge line 1
domain 2a
Hinge line 2
Marseilles
PYRENNEAN RANGE
Perpignan
domain 2b
Hinge line 3
Creus cap
LPB (domain 3)
42°N
Present-day Ebro drainage area (85 530 km²)
Saragossa
IBERIAN RANGE
Ebro Basin
CCR
Barcelona
Present-day Oceanic crust limit
domain 4
Tarragona E2
MB
Fornax-1
Benicarlo C1
VB
NBFZ
CFZ
Valencia
0
50
100 km
Datum: WGS84
Projection: Mercator 31N
0°
Nao cap
02°E
04°E

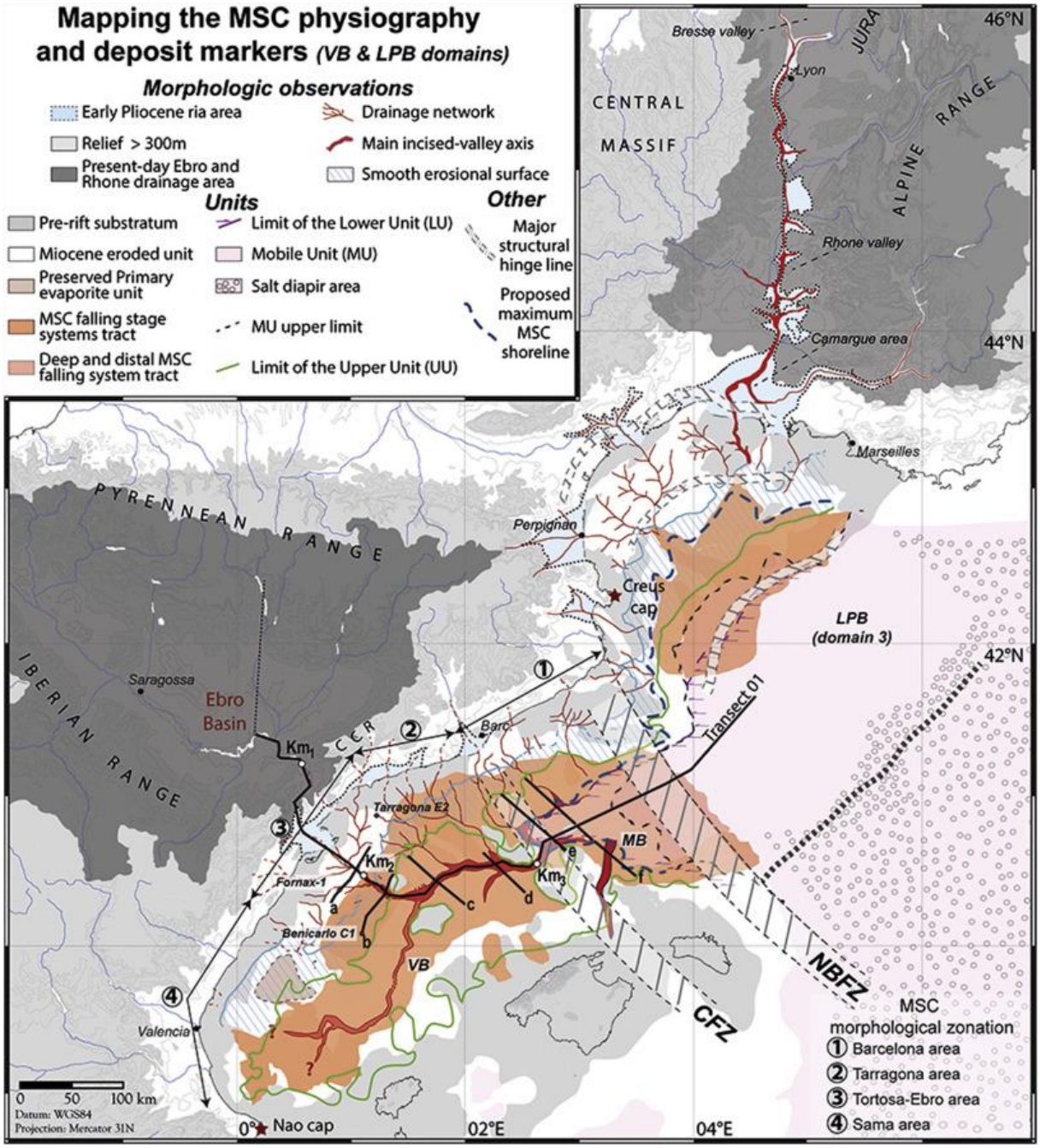
Mapping the MSC physiography and deposit markers (VB & LPB domains)
Morphologic observations
Early Pliocene ria area
Relief > 300m
Present-day Ebro and Rhone drainage area
Drainage network
Main incised-valley axis
Smooth erosional surface
Units
Pre-rift substratum
Miocene eroded unit
Preserved Primary evaporite unit
MSC falling stage systems tract
Deep and distal MSC falling system tract
Limit of the Lower Unit (LU)
Mobile Unit (MU)
Salt diapir area
MU upper limit
Limit of the Upper Unit (UU)
Other
Major structural hinge line
Proposed maximum MSC shoreline
Bresse valley
Lyon
JURA
ALPINE RANGE
CENTRAL MASSIF
Rhone valley
Camargue area
Marseilles
Perpignan
PYRENNEAN RANGE
IBERIAN RANGE
Saragossa
Ebro Basin
Creus cap
LPB (domain 3)
Barc
Transect 01
Tarragona E2
MB
Fornax-1
Benicarlo C1
VB
Valencia
NBFZ
CFZ
MSC morphological zonation
① Barcelona area
② Tarragona area
③ Tortosa-Ebro area
④ Sama area
Nao cap
0 50 100 km
Datum: WGS84
Projection: Mercator 31N
46°N
44°N
42°N
0°
02°E
04°E

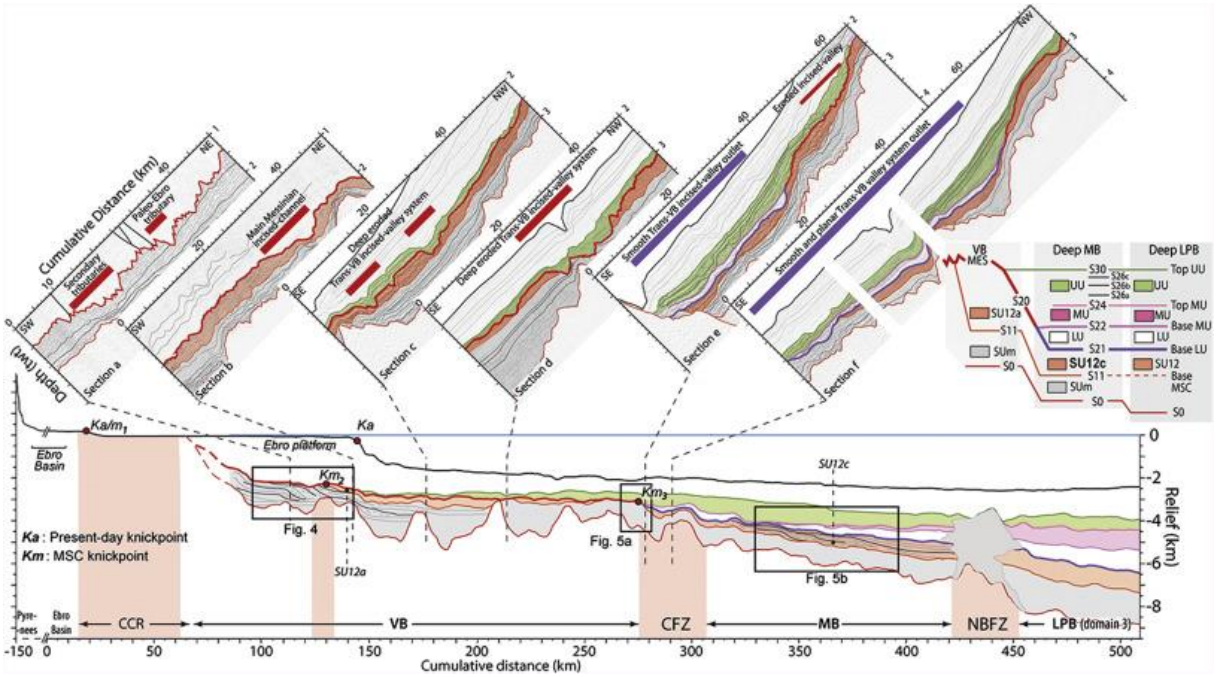
Cumulative Distance (km)
Section a
Section b
Section c
Section d
Section e
Section f
Deep MB
Deep LPB
Ka/m1
Ka
Km1
Km2
Km3
Ebro Basin
Ebro platform
SU12c
SU12a
Fig. 4
Fig. 5a
Fig. 5b
Ka : Present-day knickpoint
Km : MSC knickpoint
CCR
VB
CFZ
MB
NBFZ
LPB (domain 3)
Cumulative distance (km)
Relief (km)

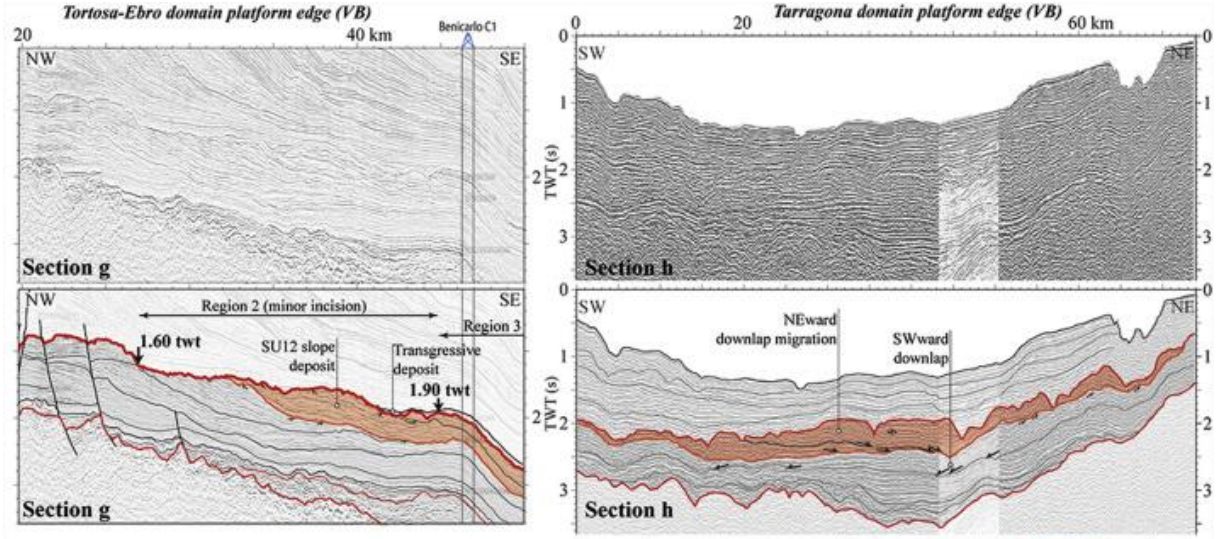
Tortosa-Ebro domain platform edge (VB)
Benicarlo C1
Section g
Region 2 (minor incision)
Region 3
1.60 twt
1.90 twt
SU12 slope deposit
Transgressive deposit
Tarragona domain platform edge (VB)
Section h
NEward downlap migration
SWward downlap
TWT (s)

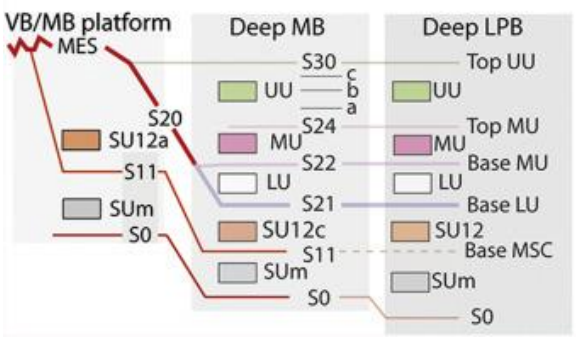
VB/MB platform
MES
Deep MB
Deep LPB
S30
Top UU
UU
S20
SU12a
S24
Top MU
MU
S11
SUm
S22
Base MU
LU
S0
S21
Base LU
SU12c
SU12
S11
Base MSC
SUm
S0

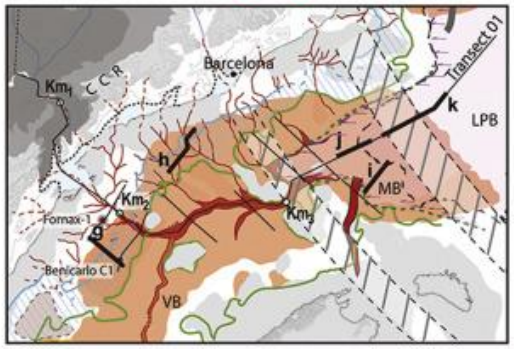
Barcelona
Transect 01
Km1
CCR
LPB
MB'
Km2
Km3
Fornax-1
Benicarlo C1
VB

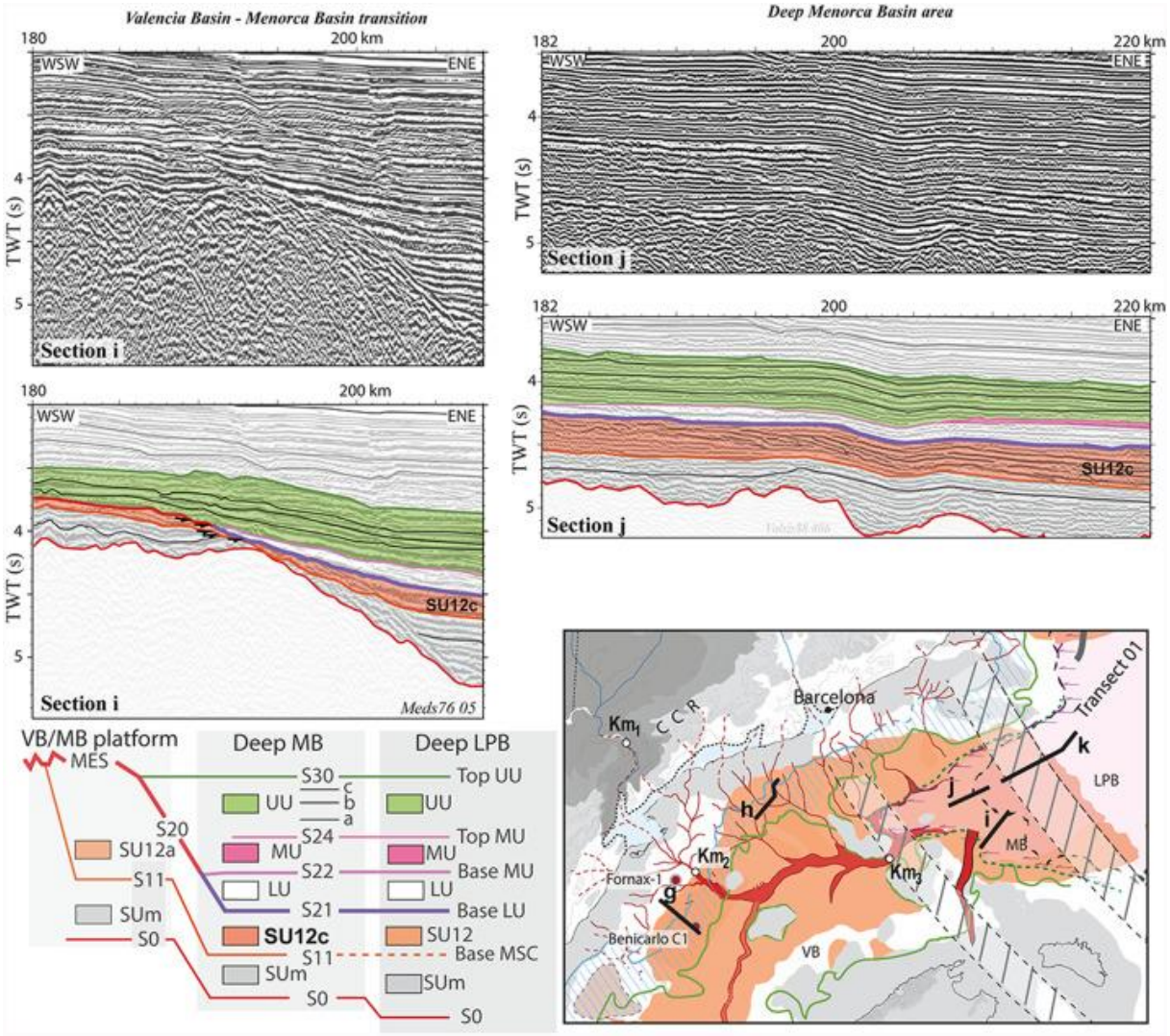
Valencia Basin - Menorca Basin transition
180
200 km
WSW
ENE
TWT (s)
4
5
Section i
SU12c
Meds76 05
Deep Menorca Basin area
182
200
220 km
Section j
VB/MB platform
MES
S20
SU12a
S11
SUm
S0
Deep MB
S30
UU
c
b
a
S24
MU
S22
LU
S21
SU12c
S11
SUm
S0
Deep LPB
Top UU
UU
Top MU
MU
Base MU
LU
Base LU
SU12
Base MSC
SUm
S0
Barcelona
Km1
C C R
Transect 01
k
j
i
h
LPB
MB
Km2
Km3
Fornax-1
g
Benicarlo C1
VB

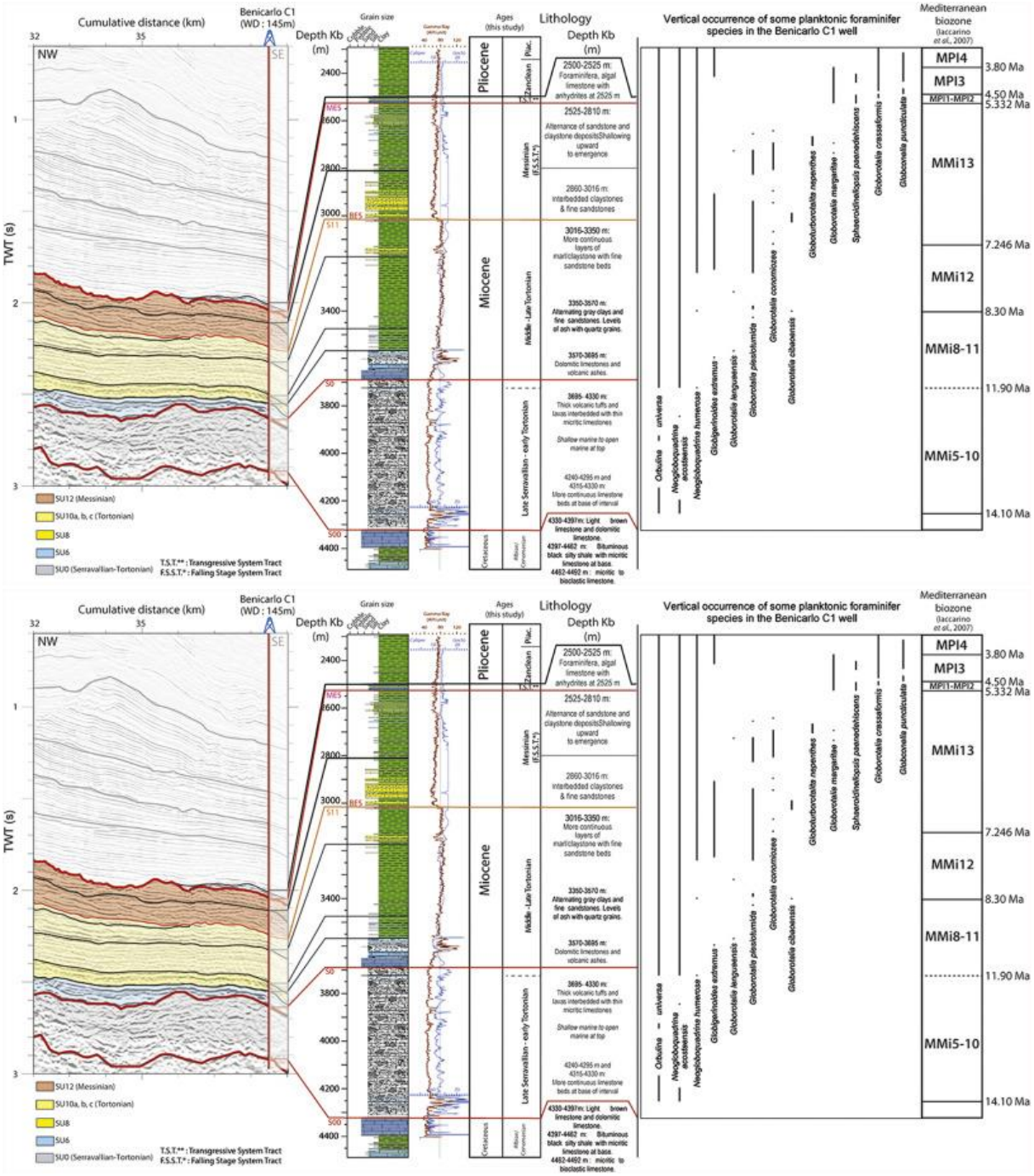
Cumulative distance (km)
Benicarlo C1
(WD : 145m)
Grain size
Ages
(this study)
Lithology
Depth Kb
(m)
Vertical occurrence of some planktonic foraminifer species in the Benicarlo C1 well
Mediterranean biozone
(Iaccarino et al., 2007)
NW
SE
TWT (s)
Pliocene
Miocene
Cretaceous
Messinian (F.S.S.T.*)
Middle - Late Tortonian
Late Serravallian - early Tortonian
Zanclean
Piac.
MES
RES
S11
S0
S00
2500-2525 m: Foraminifera, algal limestone with anhydrites at 2525 m
2525-2810 m: Alternance of sandstone and claystone depositsShallowing upward to emergence
2860-3016 m: interbedded claystones & fine sandstones
3016-3350 m: More continuous layers of marlclaystone with fine sandstone beds
3350-3570 m: Alternating gray clays and fine sandstones. Levels of ash with quartz grains.
3570-3695 m: Dolomitic limestones and volcanic ashes.
3695- 4330 m: Thick volcanic tuffs and lavas interbedded with thin micritic limestones
Shallow marine to open marine at top
4240-4295 m and 4315-4330 m: More continuous limestone beds at base of interval
4330-4397m: Light brown limestone and dolomitic limestone.
4397-4462 m: Bituminous black silty shale with micritic limestone at base.
4462-4492 m : micritic to bioclastic limestone.
Orbulina universa
Neogloboquadrina acostaensis
Neogloboquadrina humerosa
Globigerinoides extremus
Globorotalia lenguaensis
Globorotalia plesiotumida
Globorotalia conomiozea
Globorotalia cibaoensis
Globoturborotalita nepenthes
Globorotalia margaritae
Sphaeroidinellopsis paenedehiscens
Globorotalia crassaformis
Globoconella punticulata
MPI4
MPI3
MPI1-MPI2
MMi13
MMi12
MMi8-11
MMi5-10
3.80 Ma
4.50 Ma
5.332 Ma
7.246 Ma
8.30 Ma
11.90 Ma
14.10 Ma
SU12 (Messinian)
SU10a, b, c (Tortonian)
SU8
SU6
SU0 (Serravallian-Tortonian)
T.S.T.** : Transgressive System Tract
F.S.S.T.* : Falling Stage System Tract

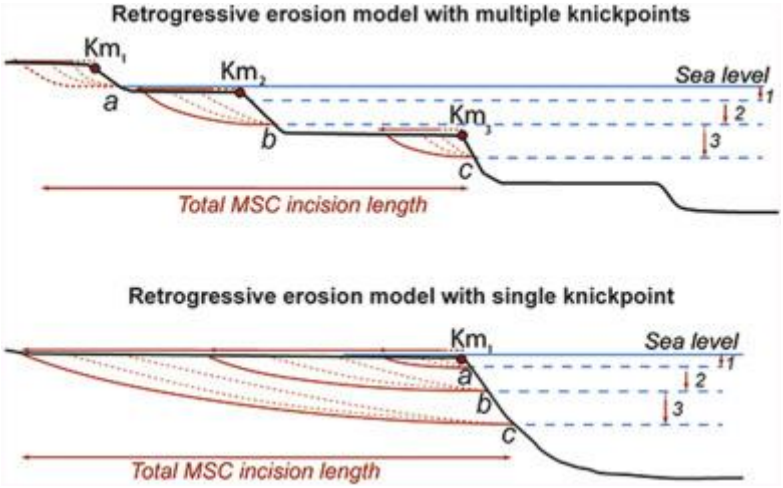
Retrogressive erosion model with multiple knickpoints
Km1
Km2
Km3
Sea level
1
2
3
a
b
c
Total MSC incision length
Retrogressive erosion model with single knickpoint
Km1
Sea level
1
2
3
a
b
c
Total MSC incision length

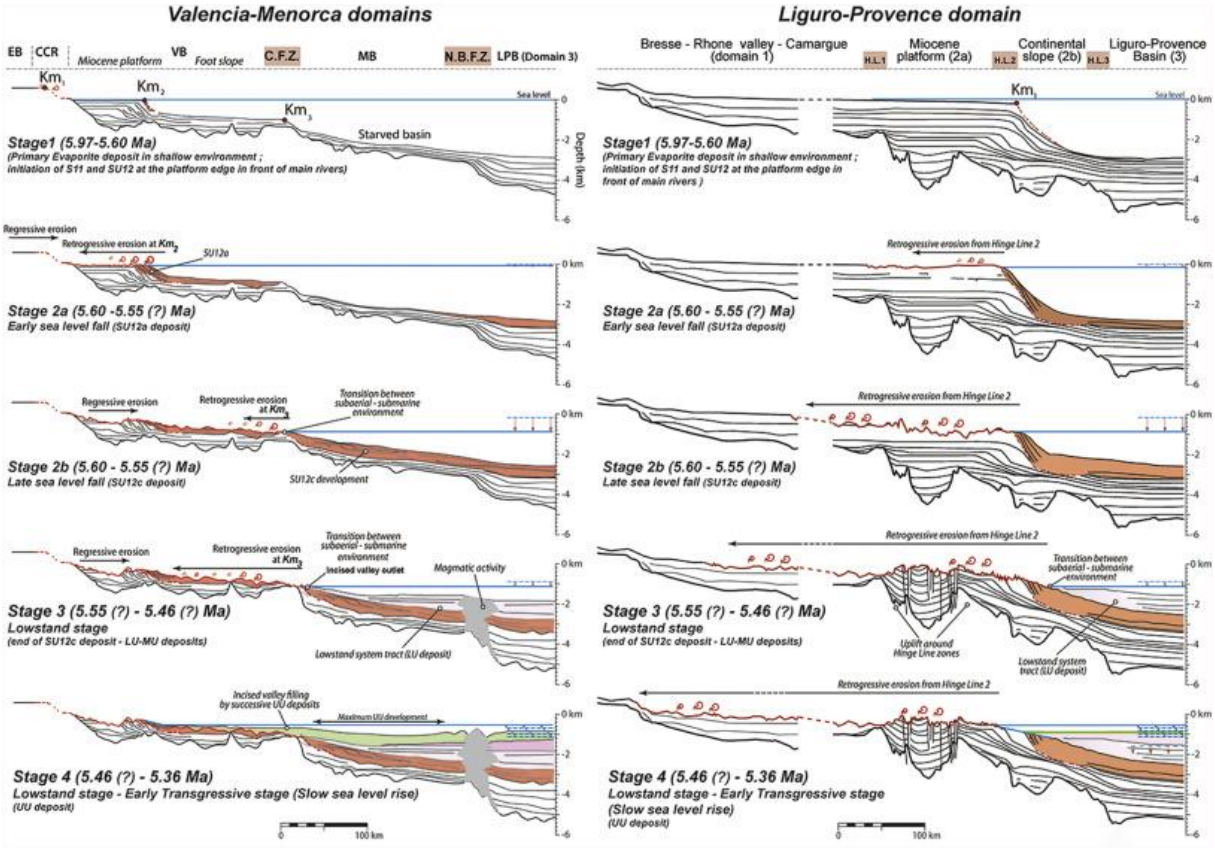
Valencia-Menorca domains
EB
CCR
Miocene platform
VB
Foot slope
C.F.Z.
MB
N.B.F.Z.
LPB (Domain 3)
Km1
Km2
Km3
Sea level
Starved basin
Depth (km)
Stage1 (5.97-5.60 Ma)
(Primary Evaporite deposit in shallow environment ; initiation of S11 and SU12 at the platform edge in front of main rivers)
Regressive erosion
Retrogressive erosion at Km2
SU12a
Stage 2a (5.60 -5.55 (?) Ma)
Early sea level fall (SU12a deposit)
Regressive erosion
Retrogressive erosion at Km2
Transition between subaerial - submarine environment
SU12c development
Stage 2b (5.60 - 5.55 (?) Ma)
Late sea level fall (SU12c deposit)
Regressive erosion
Retrogressive erosion at Km3
Transition between subaerial - submarine environment
Incised valley outlet
Magmatic activity
Lowstand system tract (LU deposit)
Stage 3 (5.55 (?) - 5.46 (?) Ma)
Lowstand stage
(end of SU12c deposit - LU-MU deposits)
Incised valley filling by successive UU deposits
Maximum UU development
Stage 4 (5.46 (?) - 5.36 Ma)
Lowstand stage - Early Transgressive stage (Slow sea level rise)
(UU deposit)
0
100 km
Liguro-Provence domain
Bresse - Rhone valley - Camargue (domain 1)
H.L.1
Miocene platform (2a)
H.L.2
Continental slope (2b)
H.L.3
Liguro-Provence Basin (3)
Km1
Km2
Km3
Sea level
Stage1 (5.97-5.60 Ma)
(Primary Evaporite deposit in shallow environment ; initiation of S11 and SU12 at the platform edge in front of main rivers)
Retrogressive erosion from Hinge Line 2
Stage 2a (5.60 - 5.55 (?) Ma)
Early sea level fall (SU12a deposit)
Retrogressive erosion from Hinge Line 2
Stage 2b (5.60 - 5.55 (?) Ma)
Late sea level fall (SU12c deposit)
Retrogressive erosion from Hinge Line 2
Transition between subaerial - submarine environment
Stage 3 (5.55 (?) - 5.46 (?) Ma)
Lowstand stage
(end of SU12c deposit - LU-MU deposits)
Uplift around Hinge Line zones
Lowstand system tract (LU deposit)
Retrogressive erosion from Hinge Line 2
Stage 4 (5.46 (?) - 5.36 Ma)
Lowstand stage - Early Transgressive stage
(Slow sea level rise)
(UU deposit)
0
100 km

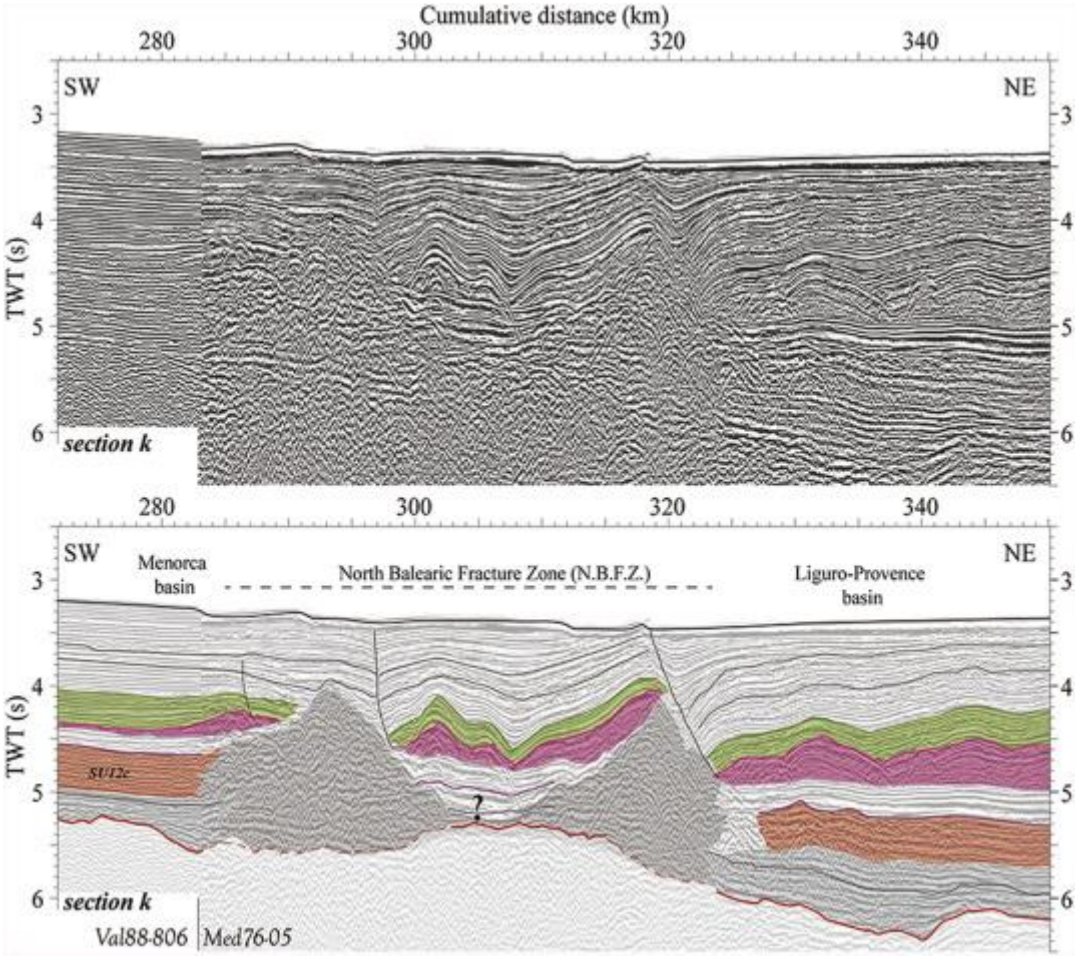

SUPPLEMENTARY MATERIAL

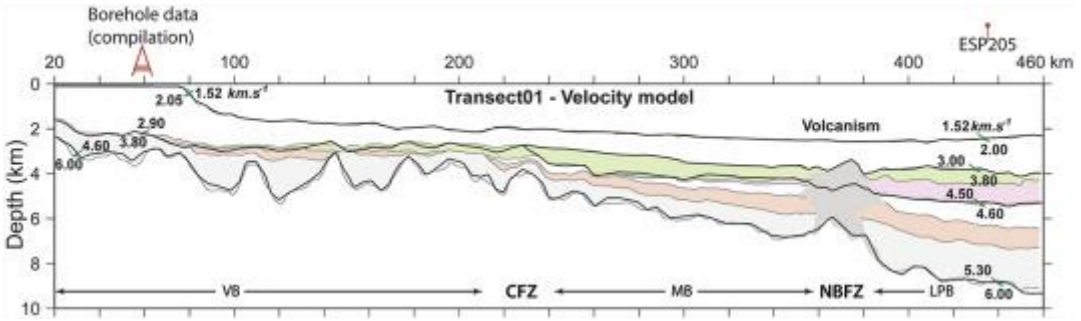

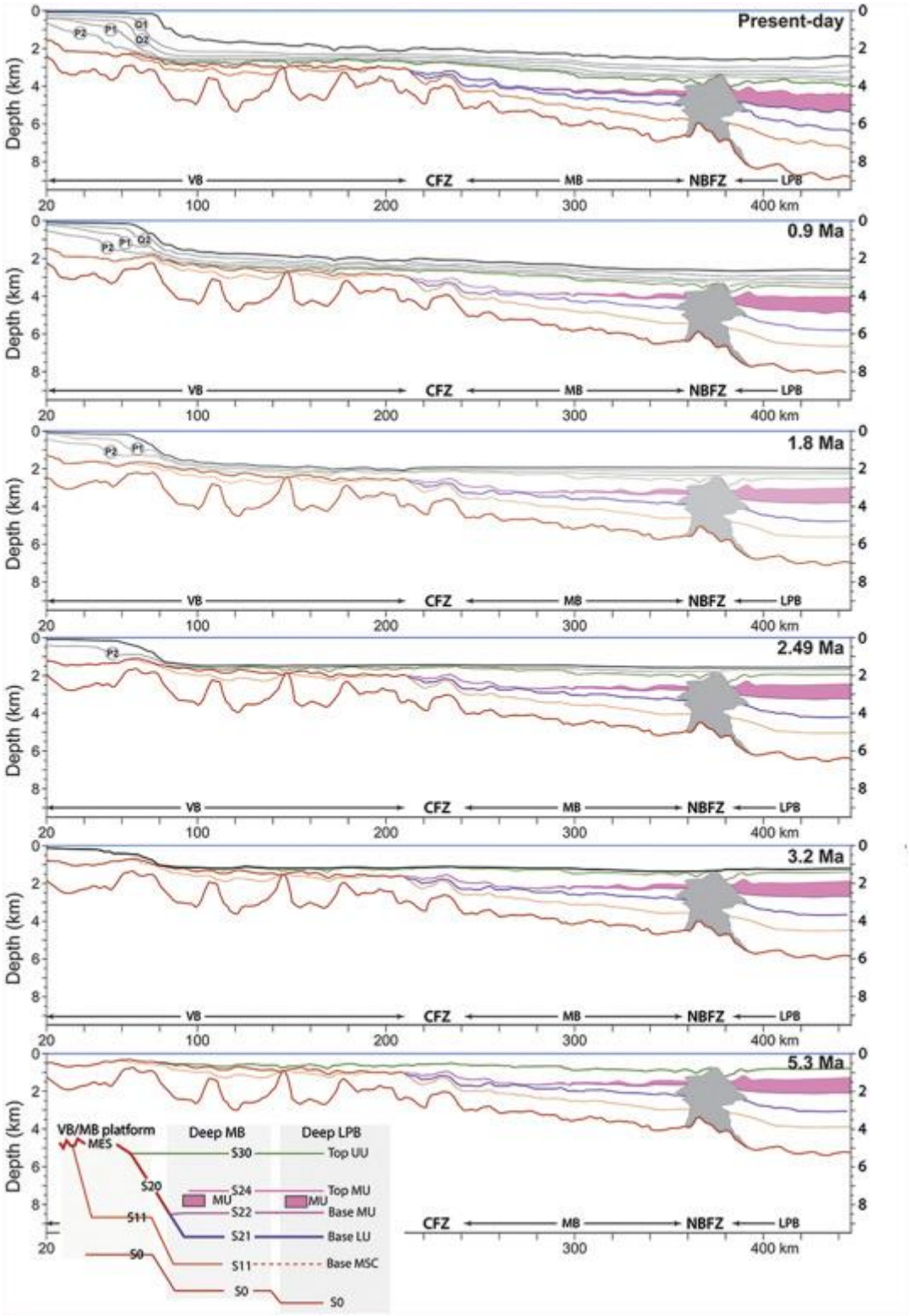
Present-day
0.9 Ma
1.8 Ma
2.49 Ma
3.2 Ma
5.3 Ma
Depth (km)
VB
CFZ
MB
NBFZ
LPB
20
100
200
300
400 km
Q1
Q2
P2
P1
VB/MB platform
MES
Deep MB
Deep LPB
S30
Top UU
S20
S24
Top MU
MU
MU
S22
Base MU
S11
S21
Base LU
S0
S11
Base MSC
S0
S0

Seismic discontinuities	Seismic unit	Seismic facies	Spatial location and observations					Age known/ supposed	Interpretations
			VB/MB Platform	VB footslope	MB footslope	MB deep basin	LPB basin (dom. 3)		
Messinian Erosional Surface (MES)		Rough erosive discontinuity	Rough erosive discontinuity until ~1.6 twt	Lateral transition to S20 and S30 at ~ 2.4-2.7 twt				Diachron surface: 5.96-5.32 Ma	Fluvial erosional surface linked to sea level fall
Ravinement Surface (RS) (Hachured blue layer)		Flat discontinuity	- MES/S30 reshaped surface - Conform with SU12 and UU units	—	—	—	—	5.46 (?) - 5.32 Ma	Marine abrasion surface (flatten by the waves)
S30		Erosive discontinuity	—	Upper lateral correlation of MES. Locally conform; high amplitude reflection				5.46 (?)- 5.32 (?) Ma	Marine erosional surface linked to sea sevel oscillation
	Upper Unit (UU) UUb, c, d	Continuous, sub-parallel reflections of medium-high amplitude	—	UUd development Filling of the incised valley	UUa,b,c,d development with erosional features	UUa, b, c, d max.development Sub-parallel horizons	UU undifferentiated unit Sub-parallel horizons	5.46 (?) - 5.32 Ma	Mixed evaporitic-detrital unit
S26a, b, c		Erosive discontinuity	—	Upper lateral correlation of MES. Locally conform; high amplitude reflection				5.46 (?) - 5.32 Ma	Marine erosional surface linked to sea sevel oscillation
	UUa	Similar as UUb, c, d	—	—	- At the Top of MU - UUa development conform to MU top unit			5.46 (?) - 5.32 Ma	Mixed evaporitic-detrital unit
S24		Mobile Unit (MU) top surface	—	—	—	Onlap on S21 (Lower Unit top surface)			
	Mobile Unit (MU)	Transparent facies	—	—	—	Full development in LPB Above LU		5.60 (?) - 5.46 (?) Ma	Halite
S22		Conform, continuous high amplitude surface	—	—	—	- MU basal surface -onlap on S21 surface			
	Lower Unit (LU)	Bedded, continuous reflectors of low frequency	—	—	—	- Initiation at Trans-VB outlet at Km3 area - Full development in LPB domain		5.60 (?) - 5.46 (?) Ma	Evaporitic or Mixed evaporitic and detrital
S21		Conform surface ; Lateral evolution of S20	—	—	—	- Slightly erosive at Km3 area - Conform with SU12c and LU			
S20		Erosive discontinuity; margin lateral correlation to MES; Basinward correlation to S21	—	- Erosive surface along trans-VB valley and paleo-relief. - Slightly erosive from either side of the incised valley.		—	—		
	SU12c (Menorca basin)	Prograding clinoform; sub-continuous with moderate amplitude reflectors	—	—	—	- Below LU unit; conformable with LU toward LPB domain; - ONO-ESE prograding trend.		5.97-5.46 (?) Ma	products of messinian erosion
	SU12a (margin)	sub-continuous with moderate amplitude reflectors; cutt and fill geometry	- Below MES and S20 - Above S11; - Bottomset reflectors	- Downstream extension limited by basement high; - Lateral transition with SU12c - SU12a troncated by SU12b		—	—	5.97-5.46 (?) Ma	Earlier marine products of messinian erosion
	SU12b (mass transport deposit) (Maillard et al., 2006)	Chaotic reflectors	—	- Below MES and S20 - Limited by the trans-VB incised valley		—	—	5.97-5.46 (?) Ma	products of messinian erosion/ link to isostatic rebound?
S11		Erosive discontinuity	- Below SU12 units;	- Below SU12 units; - Slightly erosive near paleo-relief; - Conformable surface in the MB / LPB				5.97-5.46 (?) Ma	Basal marine erosive surface
	Primary Evaporite (Del Olmo, 2011) (not show in this study)	Two continuous reflectors with medium-high amplitude	- Below MES and S20 - Only observed along the Sama area	—		—	—	5.97-5.60 Ma	Evaporitic deposit in shallow water depth